https://doi.org/10.5194/egusphere-2023-1040
Preprint. Discussion started: 1 June 2023

Retrieval of aerosol properties from zenith sky radiance measurements

Sara Herrero-Anta[1], Roberto Román[1], David Mateos[1], Ramiro González[1], Juan Carlos Antuña-Sánchez[2], Marcos Herreras-Giralda[2], Antonio Fernando Almansa[3,4], Daniel González-Fernández[1], Celia Herrero del Barrio[1], Carlos Toledano[1], Victoria E. Cachorro[1] and Ángel M. de Frutos[1].

[1]Group of Atmospheric Optics, University of Valladolid, Paseo de Belén 7, 47011 Valladolid, Spain.
[2]GRASP SAS, Remote Sensing Developments, Villeneuve D'Ascq, France
[3]Izaña Atmospheric Research Center (IARC), State Meteorological Agency of Spain (AEMET), 38001 Santa Cruz de Tenerife, Spain.
[4]Cimel Electronique, 75011 Paris, France.

Correspondence to: Sara Herrero-Anta (sara@goa.uva.es)

Abstract. This study explores the potential to retrieve aerosol properties with the GRASP algorithm (Generalized Retrieval of Atmosphere and Surface Properties) using as input measurements of zenith sky radiance (ZSR), which are sky radiances measured in the zenith direction, recorded at four wavelengths by a ZEN-R52 radiometer. To this end, the ZSR measured at 440, 500, 675 and 870 nm by a ZEN-R52 (ZSR_{ZEN}), installed in Valladolid (Spain), is employed. This instrument is calibrated intercomparing the signal of each channel with coincident ZSR values simulated (ZSR_{SIM}) at the same wavelengths with a radiative transfer model (RTM). These simulations are carried out using the GRASP forward module as RTM and the aerosol information from a collocated CE318 photometer belonging to the AERONET network (Aerosol and Robotic Network) as input. Dark signal and the signal dependence on temperature are characterized and included in the calibration process. The uncertainties on each channel are quantified by an intercomparison with a collocated CE318 photometer, obtaining lower values for shorter wavelengths; between 3% for 440 nm and 21% for 870 nm. The proposed inversion strategy for the aerosol retrieval using the ZSR_{ZEN} measurements as input, so-called GRASP-ZEN, assumes the aerosol as an external mixture of five pre calculated aerosol types. A sensitivity analysis is conducted using synthetic ZSR_{ZEN} measurements, pointing out that these measurements are sensitive to aerosol load and type. It also assesses that the retrieved aerosol optical depth (AOD) values in general overestimates the reference ones by 0.03, 0.02, 0.02 and 0.01 for 440, 500, 675, 870 nm, respectively. The calibrated ZSR_{ZEN} measurements, recorded during two and half years at Valladolid, are inverted by GRASP-ZEN strategy to retrieve some aerosol properties like AOD. The retrieved AOD shows a high correlation with respect independent values obtained from the collocated AERONET CE318 photometer, with a determination coefficient (r^2) about 0.86, 0.85, 0.79 and 0.72 for 440, 500, 675 and 870 nm, respectively, and finding uncertainties between 0.02 and 0.03 with respect to the AERONET values. Finally, it is studied the goodness of other retrieved aerosol properties like aerosol volume concentration for total, fine and coarse modes.

Keywords: zenith sky radiance, ZEN, GRASP, aerosol optical depth, AERONET, photometer

1. Introduction

Atmospheric aerosols constitute the biggest source of uncertainty in the assessment of Climate Change as assessed by Myhre et al., (2013), and yet, one decade later, not significant improvements have been made on this respect (Cissé et al., 2022). This is largely due to their high spatial and temporal variability across the globe and the complexity of its interaction with clouds (aerosol-cloud interactions) and solar radiation (aerosol-radiation interactions) (Boucher et al., 2013).

For a better understanding of aerosols and their behaviour and interactions, it is needed a high spatial and temporal monitoring coverage. Satellite measurements provides, in general, a high spatial resolution covering the whole Earth but with a low time resolution. On the other hand, some global ground-based networks, like AERONET (AErosol RObotic NETwork; Holben et al., 1998), were established to monitor aerosols around the globe. In the case of AERONET, this network counts with hundreds of stations distributed worldwide and imposes standardization of instruments, calibration, processing and distribution. The standard instrument of AERONET is CE318 photometer (Cimel Electronique SAS), which records measurements of sun (and also lunar in recent models) irradiance and sky radiance in several wavelengths. Aerosol optical depth (AOD) can be derived using the measurements of sun (or lunar if available) such as

https://doi.org/10.5194/egusphere-2023-1040
Preprint. Discussion started: 1 June 2023

in the case of AERONET, applying the Beer-Lambert-Bouguer law on the instrument's output voltage as described in Holben et al. (1998)and Giles et al. (2019). AERONET also retrieves more complex aerosol properties, like aerosol size distribution and refractive indices, using an inversion algorithm that uses as input sky radiances at different angles and wavelengths, together with the AOD values (Sinyuk et al., 2020).

Another inversion algorithm is the GRASP code (Generalized Retrieval of Atmosphere and Surface Properties; www.grasp-open.com), which is a free and open-source code that allows a flexible retrieval of aerosol properties using measurements taken from many different instruments and a combination of them (Dubovik et al., 2014; 2021). The continuous development and versatility of the code allows to explore new alternatives to apply the code to different instruments. In this sense, some authors used GRASP to retrieve aerosol properties using as input measurements, among others, of: satellites (Chen et al., 2020; Wei et al., 2021); nephelometers (Espinosa et al., 2017); multi-wavelength AOD (Torres et al., 2017); AOD and sky radiance from photometers with signal from lidars (Lopatin et al., 2013; Benavent-Oltra et al., 2017; Tsekeri et al., 2017; Molero et al., 2020) or ceilometers (Román et al., 2018; Titos et al., 2019; Herreras et al., 2019); stand-alone all-sky cameras (Román et al., 2022) and their combination with lunar photometers (Román et al., 2017) and lidar (Benavent-Oltra et al., 2019).

A new instrument that could be used for GRASP retrievals is the ZEN-R52 (Sieltec Canarias S.L.), which has already been used to retrieve AOD values by other methods (Almansa et al., 2020). The ZEN-R52 measures the zenith sky radiances (ZSR) at five different wavelengths every minute, giving continuous ZSR values during daytime at 440, 500, 675, 870 and 940 nm (this latter channel is dedicated to the study of water vapour). As advantage, this instrument has not moving parts and, in general, is cheaper than more complex photometers, which allows the installation of more instruments obtaining a higher spatial coverage. Almansa et al., (2020) presented the ZEN-R52 and developed a method to retrieve AOD values from ZSR using a lookup table (LUT) created for the site of study, Izaña (Canary Island, Spain), considering uniquely dust aerosol, which is the main aerosol type in the area due to the proximity to the Saharan desert.

In this framework, the main objective of this work is to develop a new methodology to retrieve AOD and other aerosol properties with GRASP using calibrated ZSR at 440, 500, 675 and 870 nm from a ZEN-R52 instrument. This retrieval strategy is not linked to the place of study and therefore it allows to distribute the instrument worldwide, avoiding the need to create a different LUT for each site. In addition, we propose an in-situ method for the calibration of the ZEN-R52.

The following paper is structured as follows: Section 2 gathers information regarding the instrumentation and retrieval methods employed, as well as the study location. The procedure and results of the calibration of the ZSR at the four wavelengths used is explained in Section 3, while Section 4 is used to evaluate and drive a sensitivity study of the algorithm employed for the retrieval of aerosol properties. Finally, results obtained using the proposed methodology for the retrieval of aerosol properties are shown in Section 5, and Section 6 summarizes the main conclusions of the study.

2. Data and method

2.1 Site and instrumentation

2.1.1 Valladolid GOA-UVa station

The place of study is located in Valladolid (Spain), a medium-sized city with a population of about 400000 inhabitants including the metropolitan area. The city's climate is Mediterranean (Csb Köppen–Geiger climate classification). It presents predominantly 'clean continental' aerosol with frequent episodes of Saharan desert dust intrusions, especially in summer, when the highest AOD monthly mean values are reached (Bennouna et al., 2013; Román et al., 2014; Cachorro et al., 2016).

The Group of Atmospheric Optics of the University of Valladolid (GOA-UVa) manages an instrumentation platform installed on the rooftop of the Science Faculty (41.6636° N, 4.7058° W; 705 m asl), where diverse remote sensing instruments continuously run providing complementary information about radiance, clouds, water vapour, trace gases and aerosols. Two instruments from this station are used in this work: the CE318 photometer and the ZEN-R52 radiometer. The corresponding calculations and additional information will be referred and obtained for this location.

2.1.2 CE318 photometers and AERONET products

Since 2006 the GOA-UVa has been one of the calibration facilities in charge of the calibration of AERONET standard instruments and is currently part of the European infrastructure ACTRIS (Aerosol,

https://doi.org/10.5194/egusphere-2023-1040
Preprint. Discussion started: 1 June 2023

Clouds and Trace Gases Research Infrastructure). The group is also actively contributing to the solar and moon photometry research (Barreto et al., 2019; González et al., 2020; Román et al., 2020). Due to calibration purposes, the GOA-UVa has almost always two reference AERONET photometers (masters) continuously operating on its rooftop platform for the calibration of the field instruments by intercomparison with these masters. The CE318 measures direct sun (and lunar for the recent model CE318-T; Barreto et al., 2016) irradiance at several narrow spectral bands by means of a rotating filters wheel. These direct measurements are used to derive the AOD (Giles et al., 2019) for all the available filters with and uncertainty of ±0.01 for wavelengths longer than 440 nm and ±0.02 for the UV (Holben et al., 1998). Sky radiances at several wavelengths are also measured by the CE318 on different scanning scenarios, and these sky radiances are combined with AOD values in the AERONET inversion algorithm to obtain microphysical and optical aerosol properties like aerosol volume size distribution and complex refractive index (Sinyuk et al., 2020). The sky radiances are calibrated against a calibrated integrating sphere following AERONET standards, obtaining an uncertainty of 5% for those measurements (Holben et al., 1998).

In this work, we use AOD, sky radiance values and retrieved aerosol products from inversions from AERONET version 3 level 1.5. These data have been directly downloaded from the AERONET webpage (https://aeronet.gsfc.nasa.gov), which include near-real-time automatic cloud-screening and quality control filters (level 1.5). The inversion products with a sky error above 10% have been rejected in this study to warranty the quality of the retrievals.

2.1.3 ZEN-R52

The main instrument used in this work is the ZEN-R52 radiometer, installed in the GOA-UVa platform since April 2019. Since that moment the ZEN-R52 has been continuously operating in Valladolid, except for some short malfunction periods caused by technical issues. This study uses the recorded data from April 2019 until September 2021. The device was jointly developed by Sieltec Canarias S.L. and the Izaña Atmospheric Research Center (IARC) to monitor AOD from sky radiance measurements at the zenith direction and at different spectral bands (Almansa et al., 2017; 2020). The instrument has five filters with nominal wavelengths centred at 440, 500, 675, 870 and 940 nm with a bandwidth of 10 nm and an estimated precision of ±2 nm in the central wavelength. Each filter is over a silicon diode (350–1050 nm) with a 16-bit resolution, over a high dynamic acquisition range. The 940 nm filter was recently included in this new version for precipitable water vapour retrieval but this channel is not used in this work since it is focused on aerosols. The ZEN-R52 optical configuration achieves a field of view smaller than 2º. It is equipped with a small aluminium weatherproof and protected by a thick borosilicate BK7 window, with no moving parts. All of this is mounted in such a way that the collimated sky radiance in the direction of the zenith reaches to the sensors. The instrument results to be very robust and can operate in a wide temperature range, between −40º and 85ºC. A more detailed technical description of the instrument can be found in Almansa et al. (2017; 2020).

The zenith sky radiance measurements at all channels are made simultaneously, providing an output signal in analogic-to-digital units (ADU) every minute. This output is the computed average of 30 samples taken within the minute, providing also an error (ZEN error) associated to the measurement which is the standard deviation of the 30 samples.

2.2 GRASP methodology

GRASP contains mainly two independent modules: the 'forward model' and the 'numerical inversion'. The first one is a radiative transfer model (RTM) used to simulate atmospheric remote sensing observations for a characterized atmosphere. The second module, based on the multi-term least squares method (Dubovik and King, 2000), is used in combination with the RTM for a statistically optimized fitting of the observations to retrieve aerosol properties from radiometric measurements (Dubovik et al., 2014). This provides the algorithm with high flexibility since different constrains can be applied to the retrieval and can be modified in order to adapt the retrieval to each specific situation. It is important to mention that GRASP works with normalized radiances (I_{GRASP}), which are related with the measured radiances as:

$$I_{GRASP} = I_{meas} * \pi/E_0 \qquad (1)$$

Where I_{meas} is the radiance measured by the instrument and E_0 is the extraterrestrial solar irradiance, both expressed in the same units. The standard ASTM-E490 solar spectrum has been used in this work for the normalization of Eq. (1). This spectrum was calculated for moderate solar activity and

https://doi.org/10.5194/egusphere-2023-1040
Preprint. Discussion started: 1 June 2023

medium Sun-Earth distance; therefore, it has been corrected from Sun-Earth distance for each day of the year.

2.2.1. Forward module

The GRASP forward module is a RTM based on the Succesive Orders or Scattering approach (Lenoble et al., 2007; Herreras-Giralda et al., 2022) which requires information about aerosol, gas, site coordinates and date-time together with the solar zenith angle (SZA) to characterize the atmosphere scenario. In this study gases and aerosol information are extracted from AERONET direct and inversion products available at Valladolid station. For the gases it has been used the gases optical depth (GOD), while the used aerosol information has been size distribution (in 22 log spaced bins of radius), sphere fraction and complex refractive indices at 440, 675 and 870 nm. Complex refractive index at 500 nm has been interpolated from the values at 440 and 675 nm. The bidirectional reflectance distribution function (BRDF) data is also used as input in GRASP. The used BRDF values are extracted from an 8-day climatology created for the place of study using satellite data; specifically, the MCD43C1 product from MODIS V005 collection (Schaaf et al., 2011) for the 2000–2014 period (see Román et al. 2018 for more details about these climatology values).

The ZSR has been simulated at 440, 500, 675 and 870 nm with the GRASP forward module using all the mentioned input data whenever it was available. These simulations have been used for calibration purposes as can be observed in Section 3, but also for the sensitivity analysis with synthetic data of Section 4.2. ZSR simulations are also performed for Section 4.1, but in this case the aerosol properties have been obtained for precalculated aerosol types instead of real data from AERONET.

2.2.2 Inversion strategy

The present study aims to retrieve aerosol properties with GRASP using as input the calibrated ZSR from the ZEN-R52 at four effective wavelengths. The versatility of GRASP allows different approaches to model aerosols to maximize the possibilities of the different retrieval schemes. Due to the reduced amount of information produced by the ZEN-R52, the approach called 'models' has been chosen (Chen et al., 2020). This is a simple and fast processing approach where aerosol is assumed to be an external mixture of several aerosol models. In this case the approach assumes five aerosol types which correspond to the typical aerosols on Earth: smoke, urban, oceanic, dust and urban polluted. Each model has a fixed particle size distribution, refractive indices and sphere fraction, containing the already pre-calculated phase matrix, and the extinction and absorption cross-sections (see Fig. S1 for a representation of the size distribution of each model).

This way, the inversion strategy retrieves only five independent parameters: the total aerosol volume concentration and the fraction of four models in the mixture (the fifth fraction equals one minus the rest of the fractions). All these retrieved parameters allow to obtain other complex aerosol properties, like size distribution parameters, weighting the individual properties of each model, which are known, by their fraction of the mixture. The size distribution parameters that can be obtained are volume median radius of fine (RF) and coarse (RC) modes, standard deviation of lognormal distribution for fine (σF) and coarse (σC) modes, and aerosol volume concentration for fine (VCF) and coarse (VCC) modes and the total value (VCT). AOD can be also calculated and it is given for each wavelength directly in the GRASP output. Each output, one per retrieval, provides the relative residual differences between the measured ZSR (input) and the ones generated after the inversion (simulated by GRASP forward module under the retrieved scenario) for each wavelength. This residual information will be used to evaluate the goodness of the retrievals, rejecting the non-convergent ones.

This proposed strategy requires as input: the calibrated ZSR at four wavelengths, the coordinates of the site, date, time, SZA, the BRDF values obtained from the climatology mentioned above, and the GOD at each wavelength to account for gases effect. The GOD used in this work is obtained from a monthly GOD climatology, which has been created using GOD data retrieved from AERONET for the 2012-2021 period in Valladolid. This proposed inversion strategy to retrieve aerosol properties with GRASP using ZEN-R52 measurements has been named as 'GRASP-ZEN'.

3. Calibration

https://doi.org/10.5194/egusphere-2023-1040
Preprint. Discussion started: 1 June 2023

A methodology for the ZEN-R52 calibration is proposed in this Section. This methodology is a field campaign which does not require laboratory measurements except for the dark signal characterization, and it is based on four steps: dark signal correction, quality data filtering, temperature correction, and a final comparison against simulated values to convert the output signal from ADU into radiance units ($Wm^{-2}nm^{-1}sr^{-1}$). With this purpose ZSR simulations have been performed for the whole dataset of ZEN-R52 measurements, using the GRASP forward module fed with the closest AERONET information (Section 2.2.1) whenever it was available within ±5 minutes from the ZEN-R52 measurement; considering in good approximation, and as checked later, that aerosol conditions will not change significantly within 5 minutes. Only those AERONET retrievals with a sky error lower than 5% have been used to ensure the quality of the simulations, obtaining a total of 4725 data pairs.

3.1. Dark signal correction

For the dark signal (DS) evaluation, the instrument was fully covered with a black piece and introduced into a thermal chamber in the GOA-UVa facilities. The instrument was subjected to a temperature variation in the range from -10 to 50 ºC in darkness conditions. The dark signal registered by each channel at each temperature is shown in Figure 1. It shows a constant behaviour for 440 and 500 nm filters. Contrary, for the other wavelengths a stepped exponential behaviour can be seen. In order to characterize this behaviour, the logarithm of the ZEN dark signal has been fitted to a three-degree polynomial. This fitting is after rounded up to the unit to obtain a stepped fitting. The modelled dark signal is also represented in Figure 1 by the black lines. This modelling has been used to subtract the corresponding dark signal value to the raw signal, obtaining dark signal corrected ZSR (ZSR_{DSC}). The DS signal has been characterized in the laboratory in this work in order to cover a high range of temperatures, but it could be calculated from the night-time measurements (dark sky) when a thermal chamber is no available.

3.2 Quality control filtering criteria

With the dark signal corrected, we compare the field measurements of ZSR_{DSC} against the ZSR simulated values (ZSR_{SIM}). This comparison is shown in Figure 2. The points colour in the scatter plots of Figure 2 represent the density of points per pixel as defined by Eilers and Goeman (2004), using a λ=50 for smoothness; all the density scatter plots of this paper were done with the same configuration. The determination coefficient (r^2) is also added in the panels of Figure 2, showing in general good agreement for each channel between ZSR_{DSC} and ZSR_{SIM} but with some outliers regarding the linear trend (see left panels a, c, e and g). These outliers present higher ZSR_{DSC} values than expected and they could be caused by the presence of clouds in the zenith, instrument malfunction and others.

To identify and reject the cloud-contaminated or wrong measurements, several parameters have been considered in this subsection: SZA, ZEN error, temperature, and the time interval between the inversion used to simulate the ZSR_{SIM} and the corresponding ZSR_{DSC}. Some thresholds have been identified after the visual analysis of these parameters in the scatter plot. For the SZA, the signal of ZEN instrument is higher than the expected for SZA values below 30º, which could be explained by some stray sun light coming to the sensors due to the high elevation of the Sun. Then, ZSR_{DSC} values recorded under SZA below 30º have been discarded, but also the values with SZA above 80º due to the low signal registered for this SZAs (See Figure S2 for a clear overview). The ZEN error parameter (Section 2.1.3) can be assumed as a cloud presence indicator, since measurements affected by clouds should register a high ZEN error due to the high variability of the sky radiances during the 1-min measurement. An evaluation of Figure 2 but with points classified by its ZEN error at 440 nm led us to establish a threshold of 4% for the ZEN error in the four channels (See Figure S3). If the measurement of any channel has a ZEN error above this threshold, then the measurements of the four channels are rejected.

No clear dependence of the outliers on the rest of the parameters has been observed. The results after applying the mentioned filters (30º < SZA < 80º; ZEN error < 4%) are represented in the right panels (b, d, f and h) of Figure 2. The number of coincident measurements is reduced to 4369 points after applying the quality control but a significant improvement in the determination coefficients is observed, rising from 0.96 to 0.99 for the 440nm channel and from 0.80 to 0.95 in the case of 870nm. From now on, all the ZSR_{DCS} measurements used ~~will be assumed to~~ satisfy this quality control unless specified.

3.3 Temperature correction

https://doi.org/10.5194/egusphere-2023-1040
Preprint. Discussion started: 1 June 2023

In order to check the dependence with temperature of each filter the ratio ZSR_{DSC}/ZSR_{SIM} normalized by the mean ratio is plotted against the temperature in Figure 3. In the left panels (a, c, e and g) of Figure 3 all data points are represented together with the linear fit, showing a constant behaviour for 440 and 500 nm, but a clear trend for 675 and 870 nm channels. In order to despise outliners, the ratios were grouped by 2ºC bins and its median was calculated whenever the group had at least 40 points. These median values are plotted against the mean temperature of the group's temperatures in Figure 3 right panels (b, d, f and h). The corresponding linear fit coefficients obtained in Figures 3f and 3h has been established to be used to correct the ZSR_{DSC} at 675 and 870 nm applying the next Equation 2:

$$ZSR_{TC}(\lambda) = \frac{y_{20}(\lambda)}{a(\lambda)+b(\lambda)T} ZSR_{DSC}(\lambda); \ \lambda = 675, 870\text{nm} \qquad (2)$$

where ZSR_{DSC} is the ZEN signal after dark signal correction and ZSR_{TC} is this signal with the temperature correction; a and b represent the intercept and slope of the final linear fits, respectively; y_{20} is the correspondent y-axis value of the linear fit at the temperature T of 20º C (arbitrary value chosen to normalize). This temperature correction is only applied to the λ-wavelengths of 675 and 870 nm.

3.4. Calibration coefficients

Once the dark signal correction, quality filtering and temperature correction are applied to the ZEN-R52 raw signal, the definitive comparison between the ZSR from the ZEN-R52 and the ZSR values simulated by GRASP forward module can be done to obtain the calibration coefficients. The density scatter plots between ZSR_{SIM} values and ZSR_{TC} are shown in Figure 4. The slope of the linear fit directly represents the calibration coefficients obtained to transform the ZSR_{TC} signal into radiance units ($Wm^{-2}nm^{-1}sr^{-1}$) for each channel. This calibrated radiance is named ZSR_{ZEN} hereafter.

The obtained calibration coefficients and the ones obtained by intercomparison with a calibrated integrating sphere at IARC facilities are shown in Table 1. Table 1 also presents the relative differences between both calibration coefficients using the coefficients from IARC as reference; the uncertainty involved in the latter calibration method procedure is estimated to be 5% by Walker et al. (1991) These differences are 1.39%, -6.54%, -6.72% and -5.89% for 440, 500, 675 and 870 nm, respectively. The proposed calibration method uses the standard ASTM-E490 solar spectrum for transforming the unitless output from GRASP, as indicated in Equation 1. This fact can increase the relative differences between the two calibration methods. However, the calibration method employed here allows to use the same normalization factor that lately will be applied to the ZSR_{ZEN} measurements that will be introduced in the GRASP inversion module, avoiding to introduce a systematic error due to the normalization required by the algorithm. It means that this calibration method is better suited when using the ZSR_{ZEN} values as input for GRASP to retrieve aerosol properties, since there is no need for extraterrestrial spectrum normalization. From now on ZSR_{ZEN} will stand for the calibrated zenith sky radiances measured by the ZEN-R52 satisfying the stablished quality controls (30º < SZA < 80º; ZEN error < 4%).

3.5. ZEN-R52 vs. CE318 photometer comparison

In order to check the goodness of the calibrated ZEN-R52 measurements, the ZSR_{ZEN} observations have been compared with measurements recorded by collocated CE318 instruments for the hole available dataset of ZEN-R52 measurements. For the comparison, independent measurements from CE318 photometers for two different scenarios are employed: the cloud mode (CM) and the principal plane scanning (PPL).

3.5.1. Cloud Mode

The CE318 sun-sky photometer allows to perform measurements in the 'cloud mode' scenario. It is carried out when the direct sun measurement indicates an obscured sun, and therefore the aerosol retrieval is not possible. This scenario orientates the sensor head into the zenith direction and takes zenith radiance measurements at 9 s intervals for each wavelength, which are obtained by successively rotating an interference filter in front of the detector. The 'cloud mode' scenario was originally implemented to obtain, during this idle time, cloud optical depth from zenith sky radiances at the spectral wavelengths employed by the sun-sky photometer (Chiu et al., 2010) as suggested by Marshak et al., (2000) and Barker and Marshak, (2001).

https://doi.org/10.5194/egusphere-2023-1040
Preprint. Discussion started: 1 June 2023

The zenith sky radiances measured under the cloud mode (ZSR_{CM}) have been directly downloaded from the AERONET network webpage. For the comparison with ZEN-R52, quasi-coincident (the closest within ±1 min) ZSR_{ZEN} and ZSR_{CM} measurements have been obtained and plotted in Figure 5, showing a good correlation between both datasets. The deviation between them is high, likely due to the short-time variation in the cloud radiative field. Figure 5 includes all the ZSR_{ZEN} measurements; the filtering to SZA values and ZEN errors is not applied, since the cloud mode measurements is under cloud presence. In this case, there is not dependence on SZA; outliers do not appear for SZA<30º values. Hence, the ZSR_{ZEN} values are only wrong for SZA<30º when the sun is cloud-free, which confirms the suggested explanation that ZSR_{ZEN} measurements are contaminated by stray sun light under cloud-free conditions when the sun elevation is high (SZA<30º). In addition, it was checked that 86% of the ZEN-52 measurements used in this comparison (which are known to be affected by clouds), present a ZEN error > 4% at least for one channel. This also validates the proposed use of the ZEN error as a rough 'cloud screening'.

3.5.2. Principal plane scan

CE318 sun-sky photometers allow to perform three different scanning scenarios for sky radiance measurements. One of these scanning scenarios is in the principal plane (PPL) geometry, where the azimuth angle is equal to the solar azimuth angle while the zenith angle varies measuring sky radiances at the same fixed angles regards the SZA. This is done sequentially once for each channel starting at 870nm, followed by 675, 500 and 440 nm channels for each PPL scenario. The PPL geometry allows to extract the ZSR by linear interpolation of the PPL points to the zenith position. In this situation, the cloud screening of PPL points has been made checking the smoothness of the PPL curve as described in Holben et al. (1998). The smoothness criterion analyses the second derivative of the PPL radiances with respect to the scattering angle. This way the PPL measurement is classified as cloud contaminated if the second derivative is negative (the threshold is not 0 but -1×10^{-7} as empirically determined) at any scattering angle between 2 and 90º (Almansa et al., 2020) The obtained ZSR from this method, based on the interpolation of cloud-screened CE318 sky radiances measured in the PPL geometry, has been labelled as ZSR_{PPL}.

The PPL dataset is not directly available in the AERONET webpage; then, it has been extracted from CAELIS database (Fuertes et al., 2018; González et al., 2020). ZSR_{ZEN} and ZSR_{PPL} measurements within ±1 min, are compared in Figure 6. Upper panels (a-d) of Figure 6 show the density scatter plots of ZSR_{ZEN} against the reference ZSR_{PPL}, where a high correlation between both datasets can be observed for all the channels, varying the determination coefficients from 0.94 at 870 nm to 0.99 at 440 and 500 nm. In general, the number of outliers is higher for longer wavelengths.

In order to evaluate the uncertainty of the ZSR_{ZEN} measurements using ZSR_{PPL} as reference, the relative differences between ZSR_{ZEN} and ZSR_{PPL} ($\Delta ZSR_{ZEN\text{-}PPL}$) have been evaluated and represented in frequency histograms in the bottom panels (e-h) of Figure 6. These panels also include the mean (mean bias error; MBE), median (Md) and standard deviation (SD) of $\Delta ZSR_{ZEN\text{-}PPL}$. The median values, less sensitive to outliers, are close to zero (Md = 1.36%, -1.39% and -0.22% for 440, 500 and 675 nm, respectively) indicating that the ZSR_{ZEN} are accurate regarding the reference ZSR_{PPL} values, except for 870 nm channel which Md value of 4.99% points out an overestimation of the reference ZSR values. Nevertheless, the precision decreases for longer wavelength channels, from SD values of 3.00% and 4.62% for 440 and 500 nm, respectively, to SD=12.54% and 21.37% for 675 and 870 nm.

All these statistical parameters have been calculated also considering the calibration coefficients, without temperature correction, obtained at IARC with a calibrated integrating sphere. These parameters, and the previously obtained by the proposed method of this work, are shown in Table 2 in order to observe which calibration provide ZSR values closer to the reference ZSR_{PPL} values. The results of Table 2 show that the ZSR obtained with the proposed calibration method, based on intercomparison with ZSR simulations, is in general more accurate and precise except for 440 nm. Although the results of Table 2 for 440 nm are worse for the proposed calibration than for IARC calibration, the results are still good for the proposed method with MBE close to 0 and a low value of SD. The ZSR_{ZEN} values from IARC calibration are not temperature corrected, which could be behind of part of the observed differences.

All these results indicate that the ZSR_{ZEN} at 440 and 500 nm values are more accurate and precise than at 675 and 870 nm. Then, ZSR_{ZEN} measurements at shorter wavelengths should have more weight in the aerosol retrieval than the measured for longer ones, since measurements at 440 nm and 500 nm are more trustable. The inversion module from GRASP code takes into account the weight of each measurement through the so-called 'noises'; allowing to associate a different noise to each channel in this case. Therefore,

https://doi.org/10.5194/egusphere-2023-1040
Preprint. Discussion started: 1 June 2023

the obtained standard deviation of Table 2 (using the calibration proposed in this work), associated with the ZSR_{ZEN} uncertainty, will be introduced for each channel in GRASP for the GRASP-ZEN method to account for the different reliability of each channel.

4. Sensitivity analysis

In order to analyse the capabilities of the proposed inversion strategy to invert ZSR_{ZEN} measurements with GRASP, a detailed sensitivity analysis is carried out in this section using synthetic data.

As mentioned in Section 2.2.2, the chosen method to obtain aerosols properties, considers five aerosol types or 'models', which have fixed size distribution, refractive indices and sphere fraction. The method must retrieve aerosol properties from measurements of ZSR_{ZEN} at 440, 500, 675 and 870nm. Sky radiances depend on aerosol concentration and type, among other factors like the scattering angle and SZA; hence they are commonly used to retrieve aerosol properties by measuring them at different scattering angles and wavelengths (Nakajima et al., 1996; Román et al., 2022). Figure S4 shows in the supplementary material the sky radiances in the zenith direction, modelled by GRASP for different aerosol concentrations, and how they are sensitive to changes in the AOD and aerosol type for the five aerosol types used by the inversion method. This figure shows that for higher SZA (Figure S4; panels i-l) the ZSR values are less sensitive to aerosol type and concentration, since different scenarios show smaller differences in the corresponding ZSR. Nevertheless, lower SZA conditions (Figure S4; panels a-d) show a clear sensitivity to type and aerosol load for AOD at 440nm below 0.7, that would represent and extreme AOD event (Mateos et al., 2020).

To explore the limitations of the retrieval of aerosol properties following the proposed inversion strategy, two different tests have been carried out. For both tests, artificial aerosol scenarios have been created and used as input to the GRASP forward module to simulate the ZSR that the ZEN-R52 would register under these synthetic scenarios (ZSR_{SYN}). Since the ZSR_{SYN} values are artificially created, they will be randomly perturbed following a Gaussian distribution defined by the uncertainty of each channel previously calculated for the ZEN-R52 in order to create realistic observations (similar to Torres et al., 2017 and Román et al., 2022, among others). The perturbed ZSR_{SYN} will be then used as input in the inversion module, following the GRASP-ZEN method. It will provide the retrieved aerosol properties as output, which will be labelled with the subindex 'INV' referring to 'inversion'. The test is focused on the capability to retrieve AOD values and size distribution properties.

4.1. Scenarios from the combination of five aerosol types

This test creates random synthetic aerosol scenarios formed by a mixture of the five aerosol types used by the 'models' GRASP inversion strategy (see Section 2.2.2). We aim here to assess the capabilities of the retrieval of aerosol properties if the observed aerosol is actually a pure mixture of these five types of aerosol. To this end, random fractions of each aerosol type are selected together with a random aerosol concentration chosen in the interval from 0.01 to 0.15 $\mu m^3/\mu m^2$ creating a total of 1000 scenarios. The simulations have been made for three different SZA values (30, 50 and 70°), but we will focus here in the SZA=50° situation, which would represent a half-way and common scenario for the latitude of Valladolid.

Figure 7 shows the retrieved AOD (AOD_{INV}), using as input the perturbated ZSR_{ZEN} of each created random scenario for SZA equal to 50°, against its original synthetic AOD value (AOD_{SYN}). The same graphs for SZA values of 30° and 70° are shown in the Figure S5 of the supplementary material. In general, the data deviation increases for high AOD values, which are less frequent. For SZA equal to 50°, the method overestimates the aerosol load for all the wavelengths, with MBE ranging from 0.23 to 0.11. The best results are obtained for SZA = 30°, with absolute mean bias errors lower than 0.002 for all wavelengths and the lowest uncertainty (standard deviation lower than 0.66); while for SZA = 70° the method slightly underestimates the AOD with MBEs ranging from -0.004 to 0. It is important to point out that the convergence capability of the method decreases for high SZA, being the convergent inversions a total of 43.2% and 43.6% at SZA=30° and 50° respectively but only 27.1% for SZA=70°; considering that there are initially 1000 scenarios. These results could be related to the dependence of the ZSR sensitivity on the SZA, which is higher for lower SZA, and therefore would make easier for the method to find a solution.

For the size distribution the frequency histograms of the absolute differences between the inverted and the synthetic parameters are shown in Figure 8 to have a clear overview of the results obtained (a direct scatter plot comparison is shown in Figure S6). For the current synthetic test, the retrieval of size

https://doi.org/10.5194/egusphere-2023-1040
Preprint. Discussion started: 1 June 2023

distribution properties is very accurate and precise, showing Md values very close to zero for all the properties. For the volume median radius the precision is high with SD < 10% for both fine and coarse modes, but the precision is worse for the aerosol volume concentration with an SD value about 33.2% for the total concentration. These results could be explained, at least in part, due to the fixed size distributions for the 'models', which present similar RF, RC, σF and σC values and, therefore, it will not show an important variation when combining them, but contrary, the aerosol volume concentration is an extensive property and therefore can have a higher variation.

4.2. AERONET scenarios

The same procedure than in the previous test is developed in this one but using realistic aerosol properties retrieved at Valladolid by AERONET. For this new test, all the available inversions (almucantar and hybrid scans) from AERONET for the coincident ZEN-R52 measurement period (2019-2021) with and sky error < 5% have been obtained, achieving a total of 5321 synthetic scenarios. With this test we aim to assess the capabilities of the method to retrieve the aerosol properties when the ZSR come from an aerosol scenario closer to real aerosol conditions and not necessarily to a mixture of the five mentioned aerosol types. In this situation the ZSR_{SYN} simulations are made for the corresponding date and time at which the AERONET inversion product was retrieved, achieving a wide variety of SZA values (18^o<SZA<78^o).

Figure 9 presents the comparison between the AOD_{INV}, obtained from the inversion of the perturbed ZSR_{SYN} as input in GRASP-ZEN method, and AOD_{SYN} for these AERONET synthetic scenarios. This comparison reveals a clear overestimation of the inverted AOD values compared to the original ones for the four wavelengths, ranging the MBE values from 0.01 to 0.04 and the Md from 0.01 to 0.03 for the differences between both datasets. These results could be related with the previous results for overestimated AOD at SZA = 50^o, but in this situation the overestimation is not related to the SZA since it has been checked that points with different SZA are homogeneously distributed, therefore AOD_{SYN} is always overestimated by the obtained from GRASP-ZEN for all SZA. The standard deviation of the AOD differences, which can be associated with the uncertainty in AOD_{INV}, is above 0.02, being 0.05 for 440 and 500 nm, which are higher than the standard deviation obtained in the previous section for all wavelengths and SZAs, SD = 0.090 (for AOD 440 nm at SZA=50^o).

The reason for the observed overestimation could be in the limitations of the GRASP-ZEN method based on the 'models' approach, which only allows to retrieve aerosol properties within the properties of the five aerosol types. It means that, for example, if the real aerosol has a median radius of fine mode bigger than the ones of the five 'models', then the GRASP-ZEN retrieval will underestimate the real median radius of fine mode and this difference will be compensated unbalancing other aerosol properties to fit the measured ZSR and the synthetic ZSR values of the retrieved aerosol scenario (to reduce the residual differences in ZSR values).

To explore this hypothesis, the retrieved size distribution properties have been compared with the synthetic ones. The frequency histograms for the absolute differences between the inverted and the synthetic properties are shown in Figure 10 (the direct scatter plot comparison can be seen in Figure S7). The retrieved volume concentrations present median differences regarding the synthetic ones about $0.01 \mu m^3/\mu m^2$ for VCF and VCT, while this median value is close to zero for the VCC. The retrieved fine intensive properties underestimate the reference values, being the median values of their differences about -14% and -10% for RF and σF, respectively, and -10% and -4% for RC and σC, respectively.

This lack of accuracy is the main difference between the results of Figure 10 and Figure 8. As mentioned before, we would expect a big accuracy and precision in the retrieved values of the volume median radius and standard deviation for the 'models' combination scenarios test (Section 4.1), since the scenario can be perfectly reproduced by GRASP-ZEN because it is a combination of the same models used in the inversion module; however, for a real aerosol scenario (the test for AERONET scenarios of this subsection), these properties could be impossible to obtain with enough accuracy since they present wider range of size distributions than the offered by the 'models' approach. Similar results are expected for the real and imaginary refractive index and other optical properties, due to the limitations of the 'models' approach.

The results of this section conclude that the GRASP-ZEN method is useful for the retrieval of AOD but nor for some size distribution properties, like the volume median radius and standard deviation

https://doi.org/10.5194/egusphere-2023-1040
Preprint. Discussion started: 1 June 2023

of fine and coarse modes. Therefore, we will focus on the retrieval of AOD at 440, 500, 675 and 870 nm and VCF, VCC and VCT.

5. Results

Once the ZSR_{ZEN} measurements have been obtained from ZEN-R52 by the calibration method proposed in Section 3, and the GRASP-ZEN method has been proved in Section 4 as capable to retrieve some aerosol properties like AOD, the GRASP-ZEN methodology has been applied to all the available dataset from ZEN-R52 measurements at Valladolid, obtaining a total of 222663 GRASP-ZEN retrievals. This dataset has been obtained using ZSR_{ZEN} measurements which satisfy the filtering criteria, regarding SZA and ZEN error, determined in Section 3.2. The retrievals which do not present enough convergence have been removed, which led to a total of 170637 retrievals. This convergence check is based on the residuals of the inversion process (see Section 2.2.2). A cloud-screening filter is applied, based mainly on the retrieved AOD at 500 nm, following a similar procedure as Giles et al. (2019) for cloud-screening in AERONET version 3. Three checks are applied for this cloud-screening: smoothness, stand-alone and $\pm 3\sigma$. The smoothness check is done by the analysis of the AOD variation at 500 nm: for each two subsequent values if the variation is higher than 0.01/min the retrieval with larger AOD at 500 nm in the pair is removed. After the smoothness, the stand-alone check is applied: all single retrievals remaining which are more than 1 hour apart from the closest available retrieval are removed. Finally, for each day the daily mean and standard deviation are calculated for the retrieved AOD at 500 nm and for the Ångström Exponent (AE; Ångström, 1964) obtained with the four retrieved AOD values (440, 500, 676 and 870 nm). To satisfy the $\pm 3\sigma$ check, the retrieved AOD at 500 nm and AE must be within the daily mean $\pm 3\sigma$ (triple standard deviation). Values not satisfying this requirement are removed. A final dataset with 126112 points satisfying the convergence and cloud-screening criteria is obtained.

5.1 Aerosol Optical Depth

The AOD retrieved by GRASP-ZEN using the ZSR_{ZEN} measurements (AOD_{GRASP_ZEN}) has been compared against independent AOD measurements from AERONET ($AOD_{AERONET}$) derived from CE318 sun-sky photometers collocated with the ZEN-R52 at Valladolid. Figure 11 shows the complete time series evolution of AOD_{GRASP_ZEN} together with $AOD_{AERONET}$, both at 440 nm. Despite some AOD_{GRASP_ZEN} outbreaks which are not reproduced by the $AOD_{AERONET}$, both datasets show in general a similar temporal evolution. Figure 12 shows a more detailed view of these data in a shorter period, from 16 to 22 June 2020, with high availability of data from both GRASP-ZEN and AERONET datasets for the four available wavelengths. A lack of AOD values in the GRASP-ZEN dataset around mid-day is observed; it is explained by the rejection of ZEN-R52 measurements for SZA below 30^{o}, which, in the analysed period and latitude, occurs around mid-day. In Figure 12 (panels a–d) it can be also observed that both GRASP-ZEN and AERONET datasets vary with time in a similar way for all the wavelengths, with AOD values from GRASP-ZEN slightly overestimating the AOD values from AERONET at all wavelengths. Figure 12 (panel e) includes the AOD_{GRASP_ZEN} at 440, 500, 675 and 870 nm in the same plot, showing the behaviour expected for the AOD at these wavelengths: AOD decreasing with wavelength and parallel time evolution.

To perform a more quantitative analysis of the correlation between these datasets, a match-up of AERONET AOD ($AOD_{AERONET}$) data with GRASP-ZEN AOD (AOD_{GRASP_ZEN}) values within 1.5 minutes has been made, obtaining a total of 37787 coincident points per wavelength. The AOD data from GRASP-ZEN is represented against the coincident AOD from AERONET in a density plot in Figure 13 for each wavelength (panels a- d). This figure (panels e-h) also shows in the bottom panels the frequency histograms of the differences between both AOD datasets. AOD_{GRASP_ZEN} presents a higher correlation with $AOD_{AERONET}$ for shorter wavelengths, ranging r^2 from 0.86 at 440 nm to 0.72 at 870 nm. In general, the AOD at 675 nm, and especially at 870 nm, presents more deviation between the data pairs than for the shorter wavelengths. Some outliers presenting high AOD_{GRASP_ZEN} values can be appreciated, especially at shorter wavelengths; it could be caused by some spurious measurements likely contaminated by clouds that pass the cloud-screening criteria, or recorded with dirtiness, rain droplets or dust over the instrument (it must be frequently cleaned). AOD from GRASP-ZEN generally overestimates the AERONET values, as synthetic study of Section 4.2 points out, with median values of the differences of AOD_{GRASP_ZEN} with respect to $AOD_{AERONET}$ between 0.01 and 0.02 for all wavelengths; similar values appear for MBE, ranging from 0.01 to 0.03. The uncertainty in the retrieved AOD_{GRASP_ZEN} is estimated by SD to be 0.03 for 440 and 500 nm and 0.02 for 675 and 870 nm using as reference the values provided by AERONET.

https://doi.org/10.5194/egusphere-2023-1040
Preprint. Discussion started: 1 June 2023

5.2 Aerosol volume concentration

Regarding the total aerosol volume concentration, the retrieved values with GRASP-ZEN and the obtained from AERONET along the analysed period are shown in Figure 14. The time evolution shows generally a similar behaviour for both datasets with exception of some VCT extreme values more frequent in the GRASP-ZEN database. Here it can be also seen that for this parameter there is a higher temporal coverage from GRASP-ZEN than from AERONET. This is because unlike the AOD, which is obtained from direct irradiance measurements, usually carried out every 3 minutes, the aerosol volume concentration is obtained from AERONET inversion products, which are retrieved from the combination of AOD and sky radiance measurements. Sky radiances are performed less frequently than the direct sun ones, and inversions are only processed if the sky measurements are available and satisfy certain requirements (Sinyuk et al., 2020).

The VCT, VCC and VCC values from both datasets are shown in Figure 15 for the week from 16 to 22 June 2020 (same days than Figure 12), showing again a similar behaviour for the two datasets. Figure 15 also reveals that the GRASP-ZEN values are noisier and overestimates the AERONET values, especially for the fine mode.

In order to perform a quantitative analysis for the correlation between VCT, VCC and VCC from GRASP-ZEN and AERONET datasets a match-up has been done. In this case, the GRASP-ZEN values closest to the AERONET values within 5 minutes are chosen, obtaining a total of 4356 coincident points for each volume concentration. A higher temporal range is selected here because the inversion products are less frequent than AOD. In addition, we assume that these aerosol properties should not change significantly in 5 minutes.

The GRASP-ZEN volume concentrations are represented against the coincident AERONET ones in the density scatter plots of the upper panels of Figure 16 for fine, coarse and total values. Bottom panels of Figure 16 also show the frequency histograms of the differences between GRASP-ZEN and AERONET values of VCF, VCC and VCT. The best correlation is obtained for the total volume concentration with a r^2 about 0.66, while for fine and coarse volume concentration the determination coefficient is 0.57 and 0.56, respectively. Despite the lower correlation coefficients, the retrieved volume concentrations are rather precise with values of the median of the differences between GRASP-ZEN and AERONET datasets about 0.006 and 0.005 $\mu m^3/\mu m^2$ for fine and coarse modes, respectively, and 0.010 $\mu m^3/\mu m^2$ for the VCT. The highest uncertainty on the retrieved volume concentrations is in the VCT, which presents a SD value about 0.20 $\mu m^3/\mu m^2$; while for fine and coarse modes these values are 0.009 $\mu m^3/\mu m^2$ and 0.016 $\mu m^3/\mu m^2$, which are close to the uncertainty offered by AERONET, 0.01 $\mu m^3/\mu m^2$.

All of the results of this paper have been obtained using the GRASP-ZEN methodology based on the 'models' approach, which is a suitable option for the current issue due to the reduced number of radiometric observations provided by the ZEN-R52. However, the versatility of GRASP code allows different strategies for the retrieval of aerosol properties. In this sense, we have considered other strategies in this study to choose the one which provides the best results. These strategies are based on the temporal multi-pixel approach offered by GRASP (Lopatin et al., 2021), that constraints the variation of aerosol properties in time, forcing them to vary smoothly. The multi-pixel approach was firstly used in combination with the 'models' approach. In order to avoid the problems derived of having fixed aerosol models with fixed aerosol properties, the temporal multi-pixel was also used assuming the size distribution as a bimodal (fine and coarse modes) log-normal distribution and the refractive indices have no dependence on wavelength. None of the methods improved the retrieval of aerosol properties but slightly reduce it; likely due to the intrusion of contaminated measurements that influenced the retrieval, but they did reduce the computation time (the data of a full day are inverted all at the same time). Nevertheless, these strategies could be considered for future aerosol retrievals.

6. Conclusions

This paper has explored the capabilities to calibrate a ZEN-R52 radiometer using the GRASP (Generalized Retrieval of Atmosphere and Surface Properties) code and to retrieve aerosol properties from measured zenith sky radiances (ZSR) at four wavelengths. The ZSR values measured by the ZEN-R52 radiometer for solar zenith angle (SZA) values below 30^{o} are contaminated by stray sun light intromission and, hence, should not be used. For some latitudes this would result in the absence of measurements for

https://doi.org/10.5194/egusphere-2023-1040
Preprint. Discussion started: 1 June 2023

most of the time, and therefore a technical improvement in the instrument to correct this issue is recommended to the manufacturers.

The proposed methodology for the calibration of ZEN-R52, using simulated ZSR values has been contrasted, showing discrepancies lower than 6% respect to the calibration coefficients obtained against an integrating sphere. This proposed methodology incorporates the advantage that it includes the normalization used by GRASP and therefore there is not any need to use extraterrestrial spectra to normalize the data when they are used as input in GRASP.

A new inversion strategy, called GRASP-ZEN, has been proposed to retrieve aerosol properties with GRASP code using the ZSR values measured by ZEN-R52. An analysis with synthetic data has concluded that ZSR measurements are useful to derive aerosol optical depth (AOD), since these measurements are sensitive to aerosol load and type for the ZEN-R52 channels, at least for AOD at 440 nm below 1. This sensitivity decreases when SZA increases due to the decrease on the intensity of the ZSR values. A couple of tests with synthetic data have revealed that the GRASP-ZEN inversion strategy generally overestimates the AOD for all channels under real aerosol scenarios.

The GRASP-ZEN method has been applied to ZSR measurements recorded with a ZEN-R52 radiometer at Valladolid (Spain) for two years and half. A direct comparison of some retrieved aerosol properties against independent AERONET (Aerosol Robotic Network) products has pointed out the accuracy and precision of the aerosol properties retrieved by GRASP-ZEN. The correlation between the AOD retrieved by GRASP-ZEN and AERONET is high, with determination coefficients (r^2) about 0.86, 0.85, 0.79 and 0.72 for 440, 500, 675 and 870 nm, respectively. The uncertainties on the retrieved AOD values are between $\pm$0.02 and $\pm$0.03 considering the AERONET values as reference. AERONET offers uncertainties about $\pm$0.01 for wavelengths above 440 nm, and therefore the uncertainty achieved by the proposed method is higher that the offered by the reference value.

With respect other aerosol properties, the GRASP-ZEN retrieval is limited for the intensive properties, like complex refractive index and some size distribution parameters due to the use of the 'models' approach of GRASP. Nevertheless, the retrieved volume concentrations, which are extensive properties, have been compared against the same independent AERONET products to quantify the relative accuracy and precision in these concentrations retrieved by GRASP-ZEN. The r^2 obtained comparing the volume concentrations obtained with GRASP-ZEN with respect to the AERONET reference values show low values for the fine (0.57) and coarse (0.56) modes, while for the total volume concentration a higher value (0.66) has been obtained. Nevertheless, the median and standard deviation of the differences on volume concentration between GRASP-ZEN and AERONET are lower than 0.01 $\mu m^3/\mu m^2$ and 0.02 $\mu m^3/\mu m^2$, respectively, for both fine and coarse mode and also total concentration. These results have indicated that GRASP-ZEN is capable to retrieve the aerosol volume concentrations with good accuracy and precision.

This paper shows the potential of a simple and robust radiometer like the ZEN-R52 as a possible alternative for aerosol properties retrieval in remote areas. The proposed methodology would require of a previous coincident period of measurements collocated with an AERONET CE318 photometer to achieve the calibration, and later could be deployed in a remote site in order to broaden the aerosol monitoring network. This paper also assesses the capability from GRASP to retrieve aerosol properties using only ZSR at 440, 500, 675 and 870 nm. The uncertainty and bias found in the retrieval show the limitations of the instrument and inversion strategy, but also demonstrate that the ZEN-R52, together with the developed GRASP-ZEN strategy, can provide useful information about the AOD and aerosol volume concentration for total, fine and coarse modes. This can be especially useful for remote areas or even in places with collocated a CE318 photometer in order to increase the time resolution.

https://doi.org/10.5194/egusphere-2023-1040
Preprint. Discussion started: 1 June 2023

Acknowledgments

This research has been supported by the Ministerio de Ciencia e Innovación (grant no. PID2021-127588OB-I00), the Junta de Castilla y León (grant no. VA227P20). This publication is part of the TED2021-131211B-I00 project funded by MCIN/AEI/10.13039/501100011033 and European Union "NextGenerationEU"/PRTR. This article is based upon work from COST Action CA21119 HARMONIA, supported by COST (European Cooperation in Science and Technology) and has been supported by the European Metrology Program for Innovation and Research (EMPIR) within the joint research project EMPIR 19ENV04 MAPP. We especially thank the GOA-UVa staff members (Rogelio Carracedo, Patricia Martín-Sánchez and Javier Gatón), for helping with the research through the maintenance of the instruments and the station infrastructure.

References

Almansa, A. F., Cuevas, E., Barreto, Á., Torres, B., García, O. E., García, R. D., Velasco-Merino, C., Cachorro, V. E., Berjón, A., Mallorquín, M., López, C., Ramos, R., Guirado-Fuentes, C., Negrillo, R., & de Frutos, Á. M. (2020). Column integrated water vapor and aerosol load characterization with the new ZEN-R52 radiometer. Remote Sensing, 12(9). https://doi.org/10.3390/RS12091424

Almansa, A. F., Cuevas, E., Torres, B., Barreto, Á., García, R. D., Cachorro, V. E., De Frutos, Á. M., López, C., & Ramos, R. (2017). A new zenith-looking narrow-band radiometer-based system (ZEN) for dust aerosol optical depth monitoring. Atmospheric Measurement Techniques, 10(2), 565–579. https://doi.org/10.5194/AMT-10-565-2017

Ångström, A. (1964). The parameters of atmospheric turbidity. Tellus, 16(1), 64–75. https://doi.org/10.1111/J.2153-3490.1964.TB00144.X

Barker, H. W., & Marshak, A. (2001). Inferring Optical Depth of Broken Clouds above Green Vegetation Using Surface Solar Radiometric Measurements. Journal of the Atmospheric Sciences, 58(20), 2989–3006. https://doi.org/10.1175/1520-0469(2001)058<2989:IODOBC>2.0.CO;2

Barreto, Á., Cuevas, E., Granados-Muñoz, M. J., Alados-Arboledas, L., Romero, P. M., Gröbner, J., Kouremeti, N., Almansa, A. F., Stone, T., Toledano, C., Román, R., Sorokin, M., Holben, B., Canini, M., & Yela, M. (2016). The new sun-sky-lunar Cimel CE318-T multiband photometer – A comprehensive performance evaluation. Atmospheric Measurement Techniques, 9(2), 631–654. https://doi.org/10.5194/AMT-9-631-2016

Barreto, A., Román, R., Cuevas, E., Pérez-Ramírez, D., Berjón, A. J., Kouremeti, N., Kazadzis, S., Gröbner, J., Mazzola, M., Toledano, C., Benavent-Oltra, J. A., Doppler, L., Juryšek, J., Almansa, A. F., Victori, S., Maupin, F., Guirado-Fuentes, C., González, R., Vitale, V., … Yela, M. (2019). Evaluation of night-time aerosols measurements and lunar irradiance models in the frame of the first multi-instrument nocturnal intercomparison campaign. Atmospheric Environment, 202, 190–211. https://doi.org/10.1016/J.ATMOSENV.2019.01.006

Benavent-Oltra, J. A., Román, R., Andrés Casquero-Vera, J., Pérez-Ramírez, D., Lyamani, H., Ortiz-Amezcua, P., Bedoya-Velásquez, A. E., De Arruda Moreira, G., Barreto, Á., Lopatin, A., Fuertes, D., Herrera, M., Torres, B., Dubovik, O., Luis Guerrero-Rascado, J., Goloub, P., Olmo-Reyes, F. J., & Alados-Arboledas, L. (2019). Different strategies to retrieve aerosol properties at night-time with the GRASP algorithm. Atmospheric Chemistry and Physics, 19(22), 14149–14171. https://doi.org/10.5194/ACP-19-14149-2019

Benavent-Oltra, J. A., Román, R., Granados-Munõz, M. J., Pérez-Ramírez, D., Ortiz-Amezcua, P., Denjean, C., Lopatin, A., Lyamani, H., Torres, B., Guerrero-Rascado, J. L., Fuertes, D., Dubovik, O., Chaikovsky, A., Olmo, F. J., Mallet, M., & Alados-Arboledas, L. (2017). Comparative assessment of GRASP algorithm for a dust event over Granada (Spain) during ChArMEx-ADRIMED 2013 campaign. Atmospheric Measurement Techniques, 10(11), 4439–4457. https://doi.org/10.5194/AMT-10-4439-2017

Bennouna, Y. S., Cachorro, V. E., Torres, B., Toledano, C., Berjón, A., de Frutos, A. M., & Alonso Fernández Coppel, I. (2013). Atmospheric turbidity determined by the annual cycle of the aerosol

https://doi.org/10.5194/egusphere-2023-1040
Preprint. Discussion started: 1 June 2023

optical depth over north-center Spain from ground (AERONET) and satellite (MODIS). Atmospheric Environment, 67, 352–364. https://doi.org/10.1016/J.ATMOSENV.2012.10.065

Boucher, O., Randall, D., Artaxo, P., Bretherton, C., Feingold, G., Forster, P., Kerminen, V., Kondo, Y., Liao, H., Lohmann, U., Rasch, P., Satheesh, S., Sherwood, S., Stevens, B., & Zhang, X. (2013). Clouds and Aerosols. In: Climate Change 2013: The Physical Science Basis. Contribution of Working Group I to the Fifth Assessment Report of the Intergovernmental Panel on Climate Change Coordinating Lead Authors: Lead Authors. https://doi.org/10.1017/CBO9781107415324.016

Cachorro, V. E., Burgos, M. A., Mateos, D., Toledano, C., Bennouna, Y., Torres, B., De Frutos, Á. M., & Herguedas, Á. (2016). Inventory of African desert dust events in the north-central Iberian Peninsula in 2003-2014 based on sun-photometer-AERONET and particulate-mass-EMEP data. Atmospheric Chemistry and Physics, 16(13), 8227–8248. https://doi.org/10.5194/ACP-16-8227-2016

Chen, C., Dubovik, O., Fuertes, D., Litvinov, P., Lapyonok, T., Lopatin, A., Ducos, F., Derimian, Y., Herman, M., Tanré, D., Remer, L. A., Lyapustin, A., Sayer, A. M., Levy, R. C., Christina Hsu, N., Descloitres, J., Li, L., Torres, B., Karol, Y., … Federspiel, C. (2020). Validation of GRASP algorithm product from POLDER/PARASOL data and assessment of multi-angular polarimetry potential for aerosol monitoring. Earth System Science Data, 12(4), 3573–3620. https://doi.org/10.5194/ESSD-12-3573-2020

Chiu, C. J., Huang, C.-H., Marshak, A., Slutsker, I., Giles, D. M., Holben, B. N., Knyazikhin, Y., Wiscombe, W. J., Huang, C., Marshak, A., Slutsker, I., Giles, D. M., Holben, B. N., Knyazikhin, Y., & Wiscombe, W. J. (2010). Cloud optical depth retrievals from the Aerosol Robotic Network (AERONET) cloud mode observations. Journal of Geophysical Research: Atmospheres, 115(D14), 14202. https://doi.org/10.1029/2009JD013121

Cissé, G., McLeman, R., Adams, H., Aldunce, P., Bowen, K., Campbell-Lendrum, D., Clayton, S., Ebi, K. L., Hess, J., Huang, C., Liu, Q., McGregor, G., Semenza, J., & Tirado, M. C. (2022). Health, Wellbeing, and the Changing Structure of Communities. In: Climate Change 2022: Impacts, Adaptation, and Vulnerability. Contribution of Working Group II to the Sixth Assessment Report of the Intergovernmental Panel on Climate Change [H.-O. Pörtner, D.C. Roberts, M. Tignor, E.S. Poloczanska, K. Mintenbeck, A. Alegría, M. Craig, S. Langsdorf, S. Löschke, V. Möller, A. Okem, B. Rama (eds.)]. https://doi.org/10.1017/9781009325844.008.

Dubovik, O., Fuertes, D., Litvinov, P., Lopatin, A., Lapyonok, T., Doubovik, I., Xu, F., Ducos, F., Chen, C., Torres, B., Derimian, Y., Li, L., Herreras-Giralda, M., Herrera, M., Karol, Y., Matar, C., Schuster, G. L., Espinosa, R., Puthukkudy, A., … Federspiel, C. (2021). A Comprehensive Description of Multi-Term LSM for Applying Multiple a Priori Constraints in Problems of Atmospheric Remote Sensing: GRASP Algorithm, Concept, and Applications. Frontiers in Remote Sensing, 2, 23. https://doi.org/10.3389/FRSEN.2021.706851

Dubovik, O., & King, M. D. (2000). A flexible inversion algorithm for retrieval of aerosol optical properties from Sun and sky radiance measurements. Journal of Geophysical Research: Atmospheres, 105(D16), 20673–20696. https://doi.org/10.1029/2000JD900282

Dubovik, O., Lapyonok, T., Litvinov, P., Herman, M., Fuertes, D., Ducos, F., Torres, B., Derimian, Y., Huang, X., Lopatin, A., Chaikovsky, A., Aspetsberger, M., & Federspiel, C. (2014). GRASP: a versatile algorithm for characterizing the atmosphere. SPIE Newsroom. https://doi.org/10.1117/2.1201408.005558

Eilers, P. H. C., & Goeman, J. J. (2004). Enhancing scatterplots with smoothed densities. Bioinformatics, 20(5), 623–628. https://doi.org/10.1093/BIOINFORMATICS/BTG454

Espinosa, W. R., Remer, L. A., Dubovik, O., Ziemba, L., Beyersdorf, A., Orozco, D., Schuster, G., Lapyonok, T., Fuertes, D., & Vanderlei Martins, J. (2017). Retrievals of aerosol optical and microphysical properties from Imaging Polar Nephelometer scattering measurements. Atmospheric Measurement Techniques, 10(3), 811–824. https://doi.org/10.5194/AMT-10-811-2017

https://doi.org/10.5194/egusphere-2023-1040
Preprint. Discussion started: 1 June 2023

Fuertes, D., Toledano, C., González, R., Berjón, A., Torres, B., Cachorro, V. E., & De Frutos, Á. M. (2018). CÆLIS: Software for assimilation, management and processing data of an atmospheric measurement network. Geoscientific Instrumentation, Methods and Data Systems, 7(1), 67–81. https://doi.org/10.5194/GI-7-67-2018

Giles, D. M., Sinyuk, A., Sorokin, M. G., Schafer, J. S., Smirnov, A., Slutsker, I., Eck, T. F., Holben, B. N., Lewis, J. R., Campbell, J. R., Welton, E. J., Korkin, S. V., & Lyapustin, A. I. (2019). Advancements in the Aerosol Robotic Network (AERONET) Version 3 database - Automated near-real-time quality control algorithm with improved cloud screening for Sun photometer aerosol optical depth (AOD) measurements. Atmospheric Measurement Techniques, 12(1), 169–209. https://doi.org/10.5194/AMT-12-169-2019

González, R., Toledano, C., Román, R., Fuertes, D., Berjón, A., Mateos, D., Guirado-Fuentes, C., Velasco-Merino, C., Antuña-Sánchez, J. C., Calle, A., Cachorro, V. E., & De Frutos, Á. M. (2020). Daytime and nighttime aerosol optical depth implementation in CÆLIS. Geoscientific Instrumentation, Methods and Data Systems, 9(2), 417–433. https://doi.org/10.5194/GI-9-417-2020

Herreras, M., Román, R., Cazorla, A., Toledano, C., Lyamani, H., Torres, B., Cachorro, V. E., Olmo, F. J., Alados-Arboledas, L., & de Frutos, A. M. (2019). Evaluation of retrieved aerosol extinction profiles using as reference the aerosol optical depth differences between various heights. Atmospheric Research, 230, 104625. https://doi.org/10.1016/J.ATMOSRES.2019.104625

Herreras-Giralda, M., Litvinov, P., Dubovik, O., Derimian, Y., Lapyonok, T., Fuertes, D., Sourdeval, O., Preusker, R., & Fischer, J. (2022). Thermal emission in the successive orders of scattering (SOS) radiative transfer approach. Journal of Quantitative Spectroscopy and Radiative Transfer, 291, 108327. https://doi.org/10.1016/J.JQSRT.2022.108327

Holben, B. N., Eck, T. F., Slutsker, I., Tanré, D., Buis, J. P., Setzer, A., Vermote, E., Reagan, J. A., Kaufman, Y. J., Nakajima, T., Lavenu, F., Jankowiak, I., & Smirnov, A. (1998). AERONET—A Federated Instrument Network and Data Archive for Aerosol Characterization. Remote Sensing of Environment, 66(1), 1–16. https://doi.org/10.1016/S0034-4257(98)00031-5

Lenoble, J., Herman, M., Deuzé, J. L., Lafrance, B., Santer, R., & Tanré, D. (2007). A successive order of scattering code for solving the vector equation of transfer in the earth's atmosphere with aerosols. Journal of Quantitative Spectroscopy and Radiative Transfer, 107(3), 479–507. https://doi.org/10.1016/J.JQSRT.2007.03.010

Lopatin, A., Dubovik, O., Chaikovsky, A., Goloub, P., Lapyonok, T., Tanré, D., & Litvinov, P. (2013). Enhancement of aerosol characterization using synergy of lidar and sun-photometer coincident observations: The GARRLiC algorithm. Atmospheric Measurement Techniques, 6(8), 2065–2088. https://doi.org/10.5194/AMT-6-2065-2013

Lopatin, A., Dubovik, O., Fuertes, D., Stenchikov, G., Lapyonok, T., Veselovskii, I., Wienhold, F. G., Shevchenko, I., Hu, Q., & Parajuli, S. (2021). Synergy processing of diverse ground-based remote sensing and in situ data using the GRASP algorithm: applications to radiometer, lidar and radiosonde observations. Atmospheric Measurement Techniques, 14(3), 2575–2614. https://doi.org/10.5194/AMT-14-2575-2021

Marshak, A., Knyazikhin, Y., Davis, A. B., Wiscombe, W. J., & Pilewskie, P. (2000). Cloud-vegetation interaction: Use of normalized difference cloud index for estimation of cloud optical thickness. Geophysical Research Letters, 27(12), 1695–1698. https://doi.org/10.1029/1999GL010993

Mateos, D., Cachorro, V. E., Velasco-Merino, C., O'Neill, N. T., Burgos, M. A., Gonzalez, R., Toledano, C., Herreras, M., Calle, A., & de Frutos, A. M. (2020). Comparison of three different methodologies for the identification of high atmospheric turbidity episodes. Atmospheric Research, 237, 104835. https://doi.org/10.1016/j.atmosres.2019.104835

Molero, F., Pujadas, M., & Artíñano, B. (2020). Study of the Effect of Aerosol Vertical Profile on Microphysical Properties Using GRASP Code with Sun/Sky Photometer and Multiwavelength

https://doi.org/10.5194/egusphere-2023-1040
Preprint. Discussion started: 1 June 2023

Lidar Measurements. Remote Sensing 2020, Vol. 12, Page 4072, 12(24), 4072. https://doi.org/10.3390/RS12244072

Myhre, G., Shindell, D., Bréon, F., Collins, W., Fuglestvedt, J., Huang, J., Koch, D., Lamarque, J., Lee, D., Mendoza, B., Nakajima, T., Robock, A., Stephens, G., Takemura, T., & Zhang, H. (2013). Anthropogenic and Natural Radiative Forc-ing. In: Climate Change 2013: The Physical Science Basis. Contribution of Working Group I. https://doi.org/10.1017/CBO9781107415324.018

Nakajima, T., Tonna Glauco, Rao, R., Boi, P., Kaufman, Y., & Holben, B. (1996). Use of sky brightness measurements from ground for remote sensing of particulate polydispersions. Applied Optics, Vol. 35, Issue 15, Pp. 2672-2686, 35(15), 2672–2686. https://doi.org/10.1364/AO.35.002672

Román, R., Antuña-Sánchez, J. C., Cachorro, V. E., Toledano, C., Torres, B., Mateos, D., Fuertes, D., López, C., González, R., Lapionok, T., Herreras-Giralda, M., Dubovik, O., & De Frutos, Á. M. (2022). Retrieval of aerosol properties using relative radiance measurements from an all-sky camera. Atmospheric Measurement Techniques, 15(2), 407–433. https://doi.org/10.5194/AMT-15-407-2022

Román, R., Benavent-Oltra, J. A., Casquero-Vera, J. A., Lopatin, A., Cazorla, A., Lyamani, H., Denjean, C., Fuertes, D., Pérez-Ramírez, D., Torres, B., Toledano, C., Dubovik, O., Cachorro, V. E., de Frutos, A. M., Olmo, F. J., & Alados-Arboledas, L. (2018). Retrieval of aerosol profiles combining sunphotometer and ceilometer measurements in GRASP code. Atmospheric Research, 204, 161–177. https://doi.org/10.1016/J.ATMOSRES.2018.01.021

Román, R., Bilbao, J., & de Miguel, A. (2014). Reconstruction of six decades of daily total solar shortwave irradiation in the Iberian Peninsula using sunshine duration records. Atmospheric Environment, 99, 41–50. https://doi.org/10.1016/J.ATMOSENV.2014.09.052

Román, R., González, R., Toledano, C., Barreto, Á., Pérez-Ramírez, D., Benavent-Oltra, J. A., Olmo, F. J., Cachorro, V. E., Alados-Arboledas, L., & de Frutos, Á. M. (2020). Correction of a lunar-irradiance model for aerosol optical depth retrieval and comparison with a star photometer. Atmospheric Measurement Techniques, 13(11), 6293–6310. https://doi.org/10.5194/AMT-13-6293-2020

Román, R., Torres, B., Fuertes, D., Cachorro, V. E., Dubovik, O., Toledano, C., Cazorla, A., Barreto, A., Bosch, J. L., Lapyonok, T., González, R., Goloub, P., Perrone, M. R., Olmo, F. J., de Frutos, A., & Alados-Arboledas, L. (2017). Remote sensing of lunar aureole with a sky camera: Adding information in the nocturnal retrieval of aerosol properties with GRASP code. Remote Sensing of Environment, 196, 238–252. https://doi.org/10.1016/J.RSE.2017.05.013

Schaaf, C., Liu, J., Gao, F., & Strahler, A. H. (2011). MODIS albedo and reflectance anisotropy products from Aqua and Terra, Land Remote Sensing and Global Environmental Change: NASA's Earth Observing System and the Science of ASTER and MODIS. 11, 549–561.

Sinyuk, A., Sinyuk, A., Holben, B. N., Eck, T. F., Eck, T. F., M. Giles, D., M. Giles, D., Slutsker, I., Slutsker, I., Korkin, S., Korkin, S., S. Schafer, J., S. Schafer, J., Smirnov, A., Smirnov, A., Sorokin, M., Sorokin, M., & Lyapustin, A. (2020). The AERONET Version 3 aerosol retrieval algorithm, associated uncertainties and comparisons to Version 2. Atmospheric Measurement Techniques, 13(6), 3375–3411. https://doi.org/10.5194/AMT-13-3375-2020

Titos, G., Ealo, M., Román, R., Cazorla, A., Sola, Y., Dubovik, O., Alastuey, A., & Pandolfi, M. (2019). Retrieval of aerosol properties from ceilometer and photometer measurements: Long-term evaluation with in situ data and statistical analysis at Montsec (southern Pyrenees). Atmospheric Measurement Techniques, 12(6), 3255–3267. https://doi.org/10.5194/AMT-12-3255-2019

Torres, B., Dubovik, O., Fuertes, D., Schuster, G., Eugenia Cachorro, V., Lapyonok, T., Goloub, P., Blarel, L., Barreto, A., Mallet, M., Toledano, C., & Tanré, D. (2017). Advanced characterisation of aerosol size properties from measurements of spectral optical depth using the GRASP algorithm. Atmospheric Measurement Techniques, 10(10), 3743–3781. https://doi.org/10.5194/AMT-10-3743-2017

https://doi.org/10.5194/egusphere-2023-1040
Preprint. Discussion started: 1 June 2023

Tsekeri, A., Lopatin, A., Amiridis, V., Marinou, E., Igloffstein, J., Siomos, N., Solomos, S., Kokkalis, P., Engelmann, R., Baars, H., Gratsea, M., Raptis, P. I., Binietoglou, I., Mihalopoulos, N., Kalivitis, N., Kouvarakis, G., Bartsotas, N., Kallos, G., Basart, S., … Dubovik, O. (2017). GARRLiC and LIRIC: strengths and limitations for the characterization of dust and marine particles along with their mixtures. Atmospheric Measurement Techniques, 10(12), 4995–5016. https://doi.org/10.5194/AMT-10-4995-2017

Walker, J. H., Cromer, C. L., & McLean, J. T. (1991). Calibration of passive remote observing optical and micrwave instrumentation. Proc. SPIE—The International Soc. of Optical Engineering, 3–5 April, Orlando, FL, 1493, 224–230.

Wei, Y., Li, Z., Zhang, Y., Chen, C., Xie, Y., Lv, Y., & Dubovik, O. (2021). Derivation of PM10 mass concentration from advanced satellite retrieval products based on a semi-empirical physical approach. Remote Sensing of Environment, 256, 112319. https://doi.org/10.1016/J.RSE.2021.112319

List of Tables

Table 1. Calibration coefficients obtained using simulations of zenith sky radiance (Coef-SIM) and the ones obtained at the IARC against a calibrated integrating sphere (Coef-IARC). The relative difference (Δ) between both coefficients is included assuming Coef-IARC as reference.

λ (nm)	Coef – SIM (W/m^2nmsr)	Coef- IARC (W/m^2nmsr)	Δ (%)
440	3.2928e-05	3.2485e-05	1.39
500	1.1426e-05	1.2223e-05	-6.54
675	2.0734e-05	2.2221e-05	-6.72
870	1.6840e-05	1.7901e-05	-5.89

Table 2. Determination coefficient (r^2) between ZSR_{ZEN} and ZSR_{PPL} and the mean (MBE), median (Md) and standard deviation (SD) of the Δ differences between ZSR_{ZEN} and ZSR_{PPL} at 440nm, 500nm, 675 nm and 870 nm using the calibration coefficient obtained in this paper with simulated ZSR values and the ones obtained with an integrating sphere at IARC in parenthesis. N represents the number of coincident ZSR_{ZEN} and ZSR_{PPL} data pairs.

	λ (nm)	r^2	MBE (%)	SD (%)	Md (%)	N
This paper (IARC)	**440**	0.99 (0.99)	1.96 (0.73)	3.00 (2.95)	1.36 (0.16)	1327
	500	0.99 (0.99)	-0.34 (6.67)	4.62 (4.95)	-1.39 (5.56)	1317
	675	0.95 (0.95)	3.76 (14.67)	12.54 (13.92)	-0.22 (10.96)	1289
	870	0.94 (0.94)	10.56 (26.67)	21.37 (25.13)	4.99 (20.96)	1165

List of Figures

https://doi.org/10.5194/egusphere-2023-1040
Preprint. Discussion started: 1 June 2023

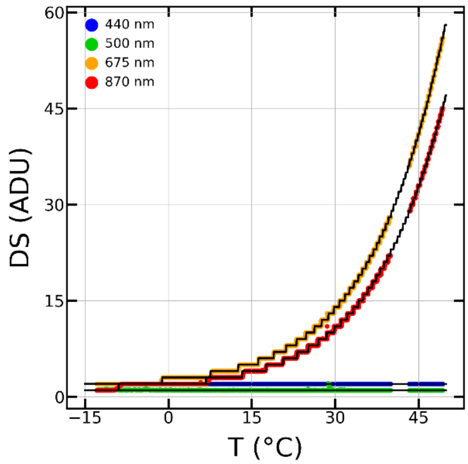

Figure 1. ZEN-R52 dark signal (DS) in analogic-to-digital units (ADU) against the temperature (coloured dots) at 440, 500, 675 and 870 nm. Black lines represent the DS for each channel.

https://doi.org/10.5194/egusphere-2023-1040
Preprint. Discussion started: 1 June 2023

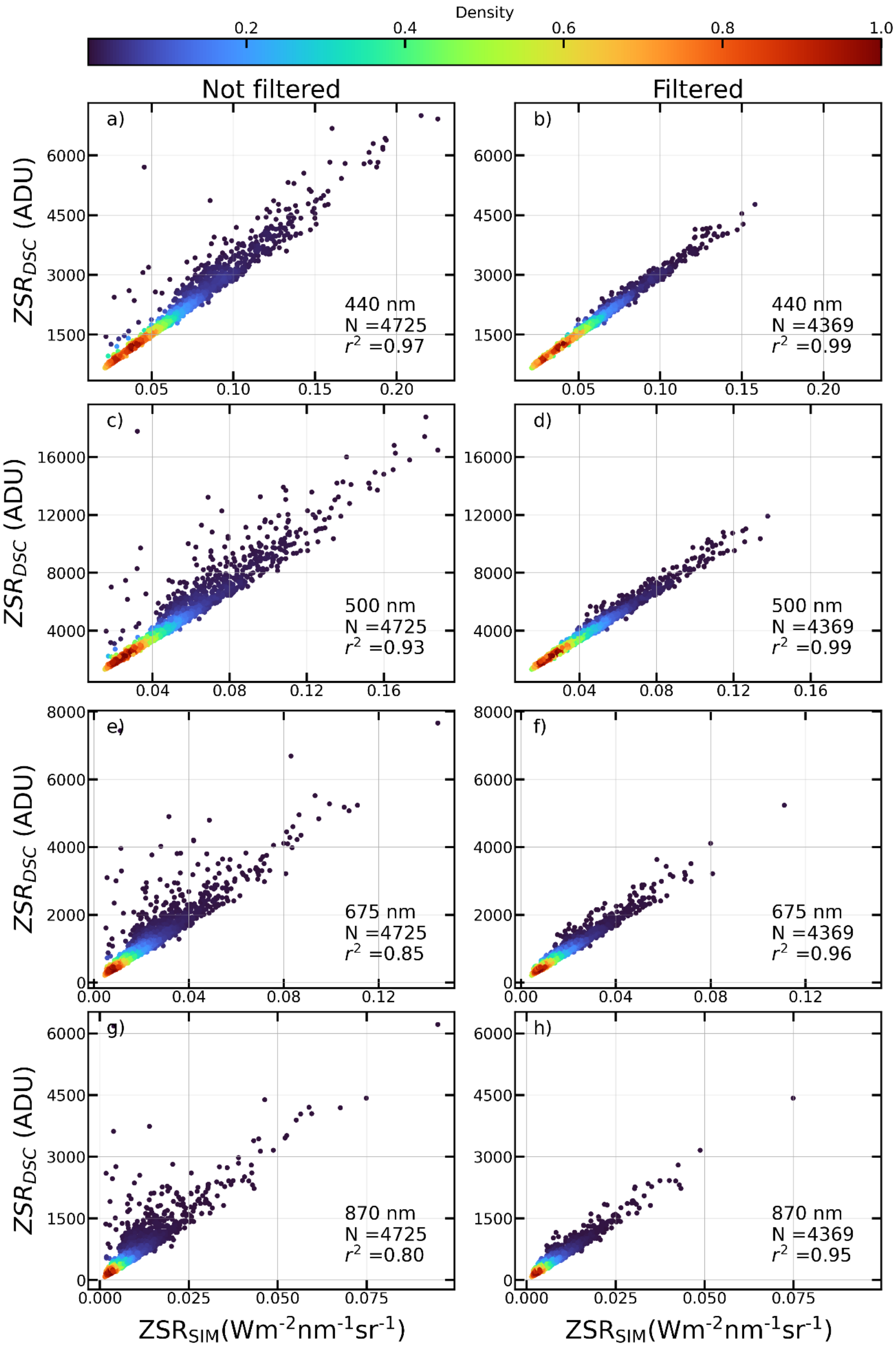

Figure 2. Density scatter plot of the measured zenith sky radiances corrected from dark signal (ZSR_{DSC}), in analogic-to-digital units (ADU), against the zenith sky radiances simulated by GRASP (ZSR_{SIM}), both at 440 nm (upper panels), 500 nm (second row panels), 675 nm (third row panels) and 870 nm (bottom panels). Left and right panels show these data before and after applying a quality control filtering, respectively. Determination coefficient (r^2) and number of data pairs (N) are also shown.

https://doi.org/10.5194/egusphere-2023-1040
Preprint. Discussion started: 1 June 2023

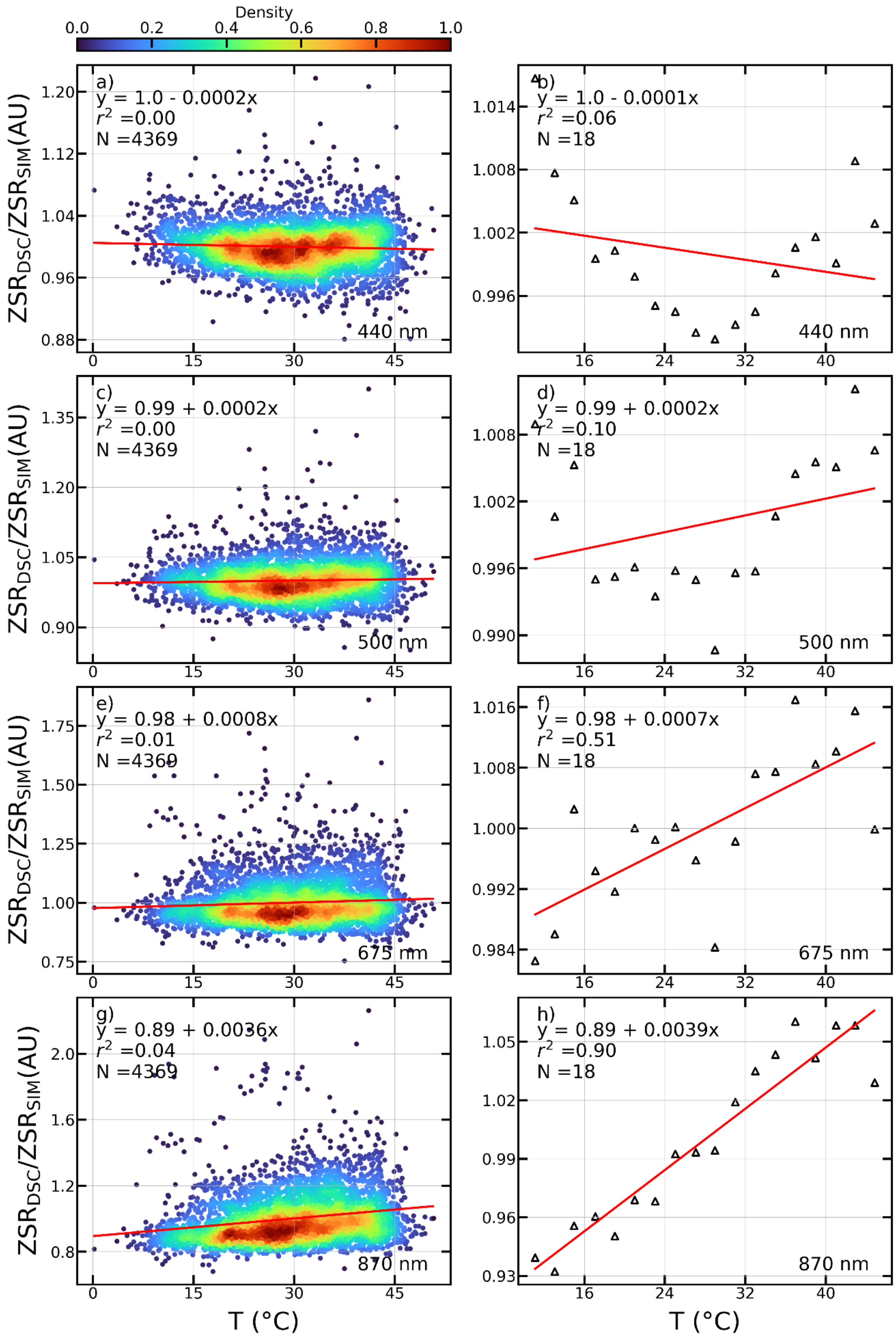

Figure 3. Left panel. density scatter plots for the normalized ratios ZSR_{DSC}/ZSR_{SIM} in arbitrary units (AU) against the temperature at a) 440nm, c) 500nm, e) 675 nm and g) 870 nm. Right panel. scatter plot of the median value for the ratios ZSR_{DSC}/ZSR_{SIM} grouped in 2°C ranges against mean temperature of the group at b) 440nm,

https://doi.org/10.5194/egusphere-2023-1040
Preprint. Discussion started: 1 June 2023

d) 500nm, f) 675 nm and h) 870 nm. Linear fit (red line), determination coefficient (r^2) and its equation and number of data points (N) are also shown.

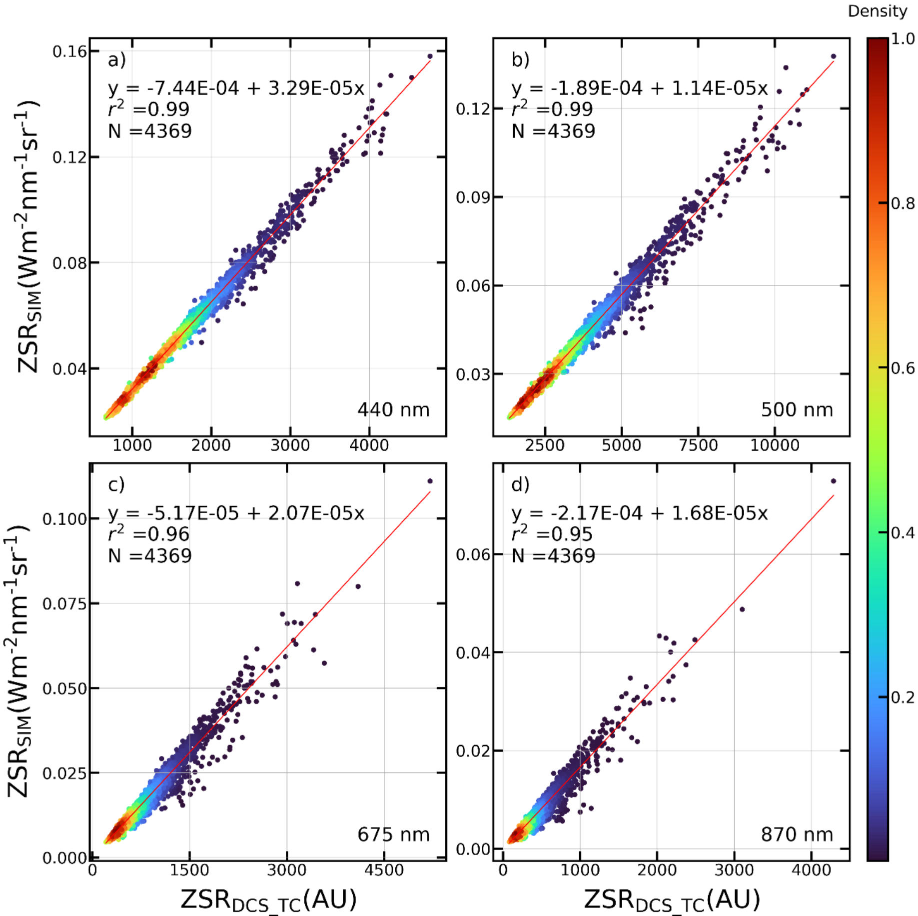

Figure 4. Density scatter plot of the zenith sky radiance simulated (ZSR_{SIM}) in radiance units against the ZEN-R52 measurements in arbitrary units (AU) corrected in dark signal and temperature (ZSR_{DSC_TC}) at a) 440nm, b) 500nm, c) 675 nm and d) 870 nm. Linear fit (red line) and its equation, determination coefficient (r^2) and number of data points (N) are also shown.

https://doi.org/10.5194/egusphere-2023-1040
Preprint. Discussion started: 1 June 2023

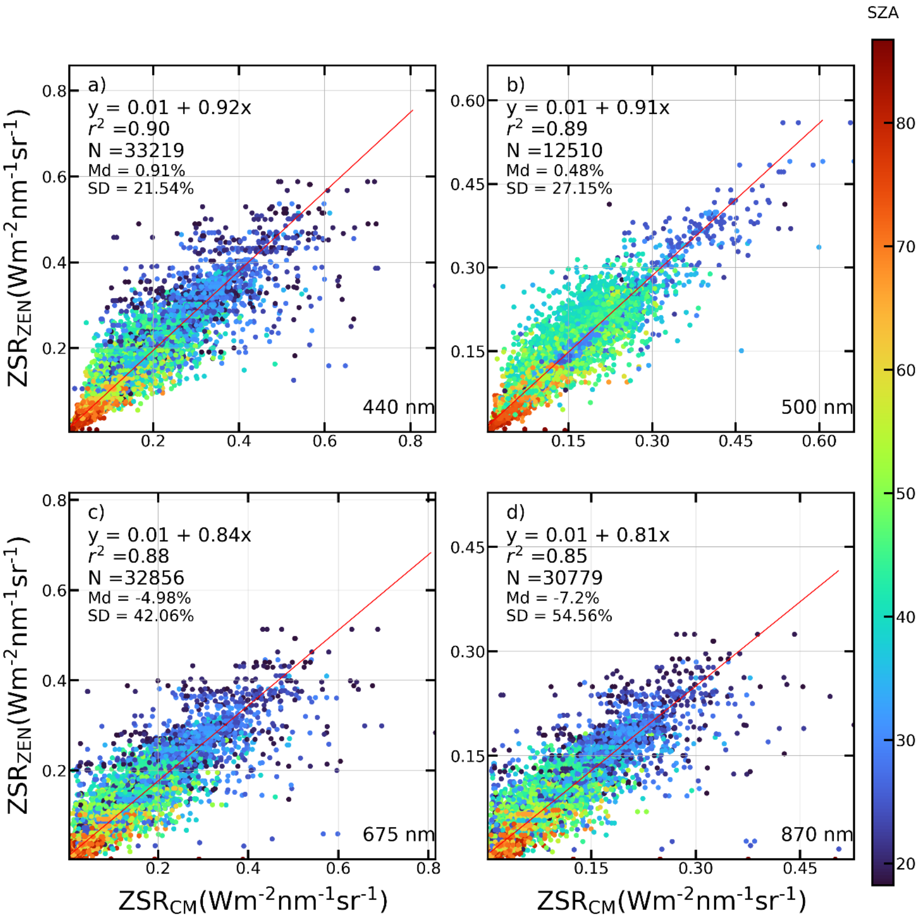

Figure 5. Scatter plot of the calibrated ZEN-R52 measurements (ZSR_{ZEN}) against coincident measurements from AERONET Cloud Mode (ZSR_{CM}) at a) 440nm, b) 500nm, c) 675 nm and d) 870 nm. Linear fit (red line) and its equation, determination coefficient (r2) and number of data points (N) are shown. The median (Md) and standard deviation (SD) of the Δ differences are also shown. Points colours represent the SZA.

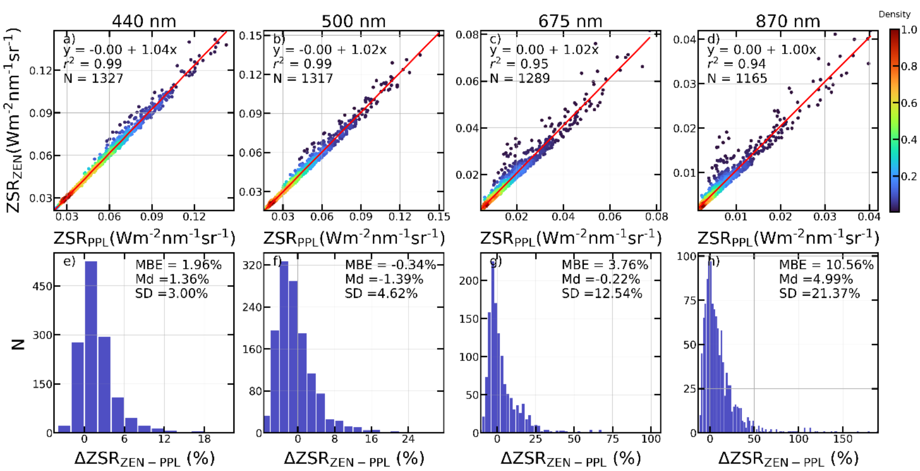

https://doi.org/10.5194/egusphere-2023-1040
Preprint. Discussion started: 1 June 2023

Figure 6. (a-d) Density scatter plot of the calibrated ZEN-R52 measurements (ZSR_{ZEN}) against coincident zenith sky radiances derived from AERONET PPL measurements ($ZSR_{ZEN-PPL}$) at a) 440 nm, b) 500 nm, c) 675 nm and d) 870 nm. Linear fit (red line), its equation, determination coefficient (r^2) and number of data pairs (N) are shown. (e-h) Frequency histograms of the $\Delta ZSR_{ZEN-PPL}$ differences in AOD from ZEN-R52 and AERONET PPL e) 440 nm, f) 500 nm, g) 675 nm and h) 870 nm. The mean bias error (MBE), median (Md) and standard deviation (SD) of the differences are also shown.

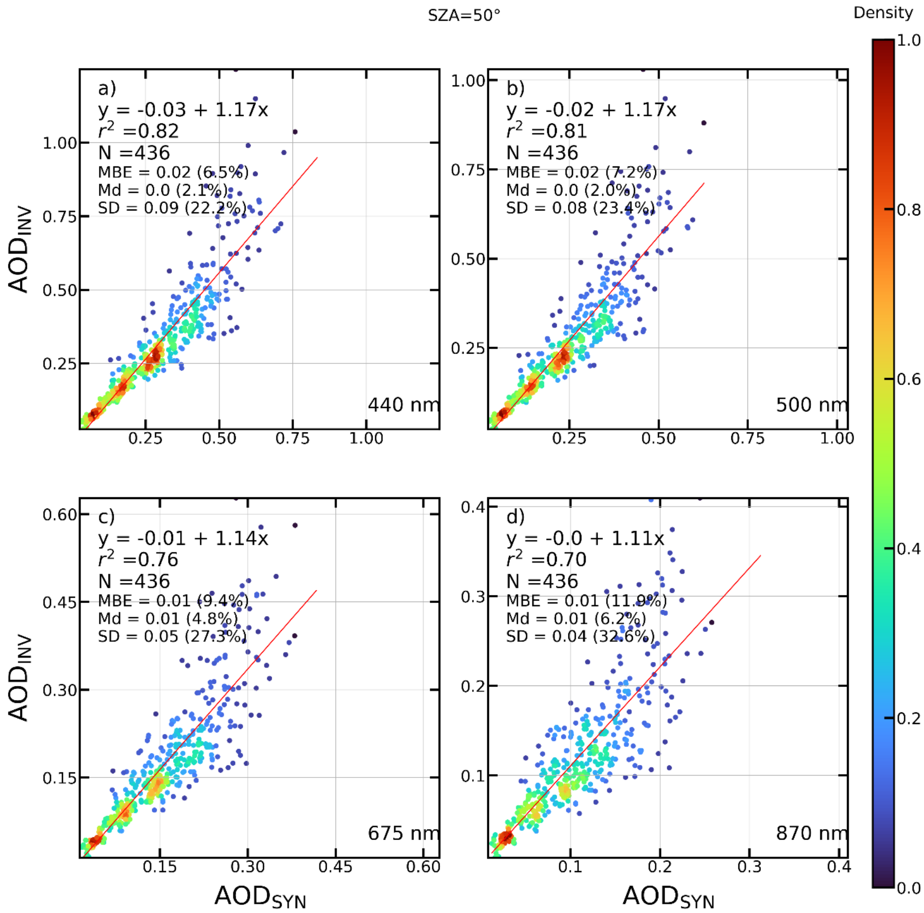

Figure 7. Density scatter plot of the AOD retrieved by GRASP after the inversion of synthetic ZSR (AOD_{INV}) against the initial AOD (AOD_{SYN}) obtained for synthetic scenarios created from the combination of five aerosol types for SZA=50° at a) 440nm, b) 500nm, c) 675 nm and d) 870 nm. Linear fit (red line) with its equation, determination coefficient (r^2) and number of data points (N) are shown. Mean bias error (MB), median (Md) and standard deviation (SD) of the absolute and Δ (between brackets) differences between the inverted and synthetic AOD are also included.

https://doi.org/10.5194/egusphere-2023-1040
Preprint. Discussion started: 1 June 2023

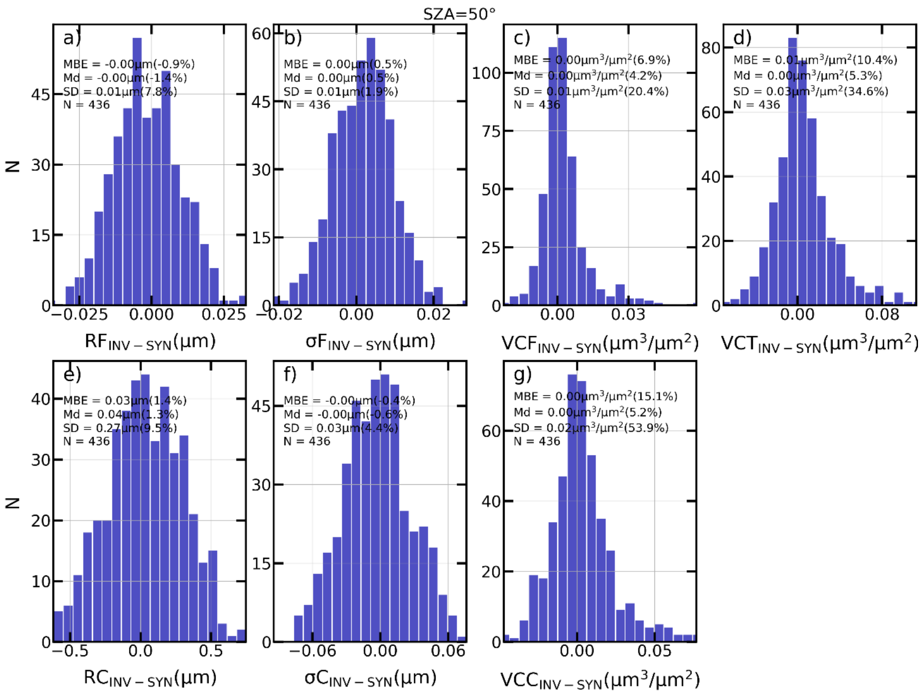

Figure 8. Frequency histograms of the absolute differences in the aerosol size distribution properties retrieved by GRASP after the inversion of synthetic ZSR (INV) and the ones initially obtained (SYN) for synthetic scenarios created from the combination of five aerosol types at SZA=50º. The mean bias error (MBE), median (Md) and standard deviation (SD) and their corresponding value for the Δ differences (between brackets) are also shown. These size distribution properties are volume median radius of fine (RF) and coarse (RC) modes, standard deviation of log-normal distribution for fine (σF) and coarse modes (σC), and aerosol volume concentration for fine (VCF) and coarse (VCC) modes and the total (VCT).

https://doi.org/10.5194/egusphere-2023-1040
Preprint. Discussion started: 1 June 2023

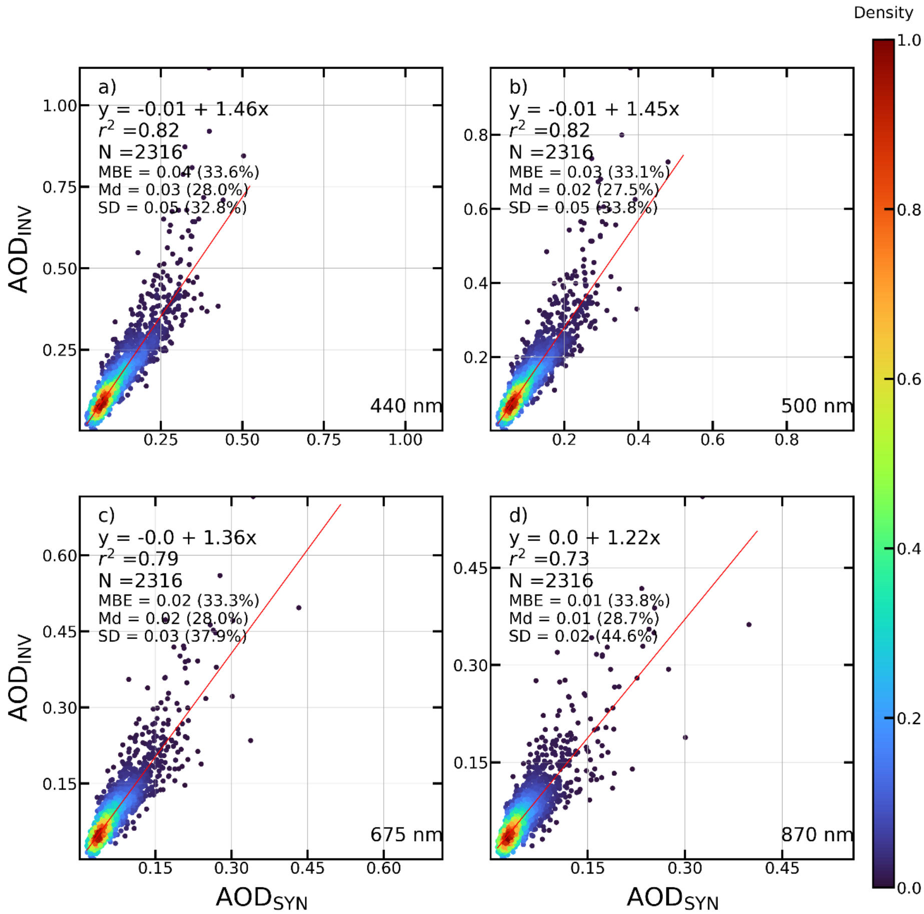

Figure 9. Density scatter plot of the AOD retrieved by GRASP after the inversion of synthetic ZSR (AOD_{INV}) against the initial AOD (AOD_{SYN}) obtained for synthetic scenarios created from AERONET retrievals at a) 440nm, b) 500nm, c) 675 nm and d) 870 nm. Linear fit (red line) with its equation, determination coefficient (r^2) and number of data points (N) are shown. Mean bias error (MB), median (Md) and standard deviation (SD) of the absolute and Δ (between brackets) differences between the inverted and synthetic AOD are also included.

https://doi.org/10.5194/egusphere-2023-1040
Preprint. Discussion started: 1 June 2023

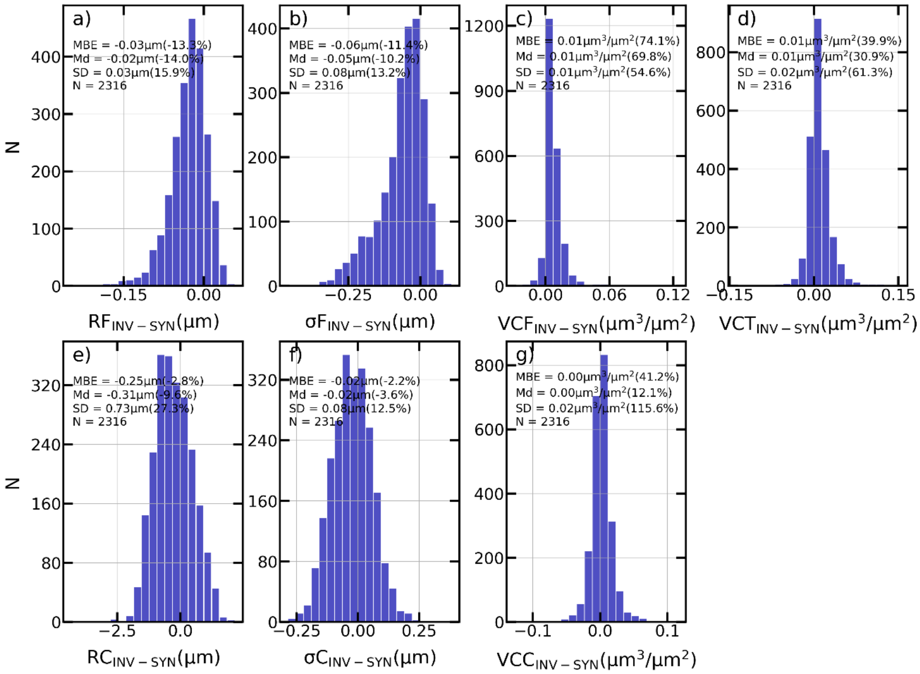

Figure 10. Frequency histograms of the absolute differences in the aerosol size distribution properties retrieved by GRASP after the inversion of synthetic ZSR (INV) and the ones initially obtained (SYN) for synthetic scenarios created from AERONET retrievals. The mean bias error (MBE), median (Md) and standard deviation (SD) and their corresponding value for the Δ differences (between brackets) are also shown. These size distribution properties are volume median radius of fine (RF) and coarse (RC) modes, standard deviation of log-normal distribution for fine (σF) and coarse modes (σC), and aerosol volume concentration for fine (VCF) and coarse (VCC) modes and the total (VCT).

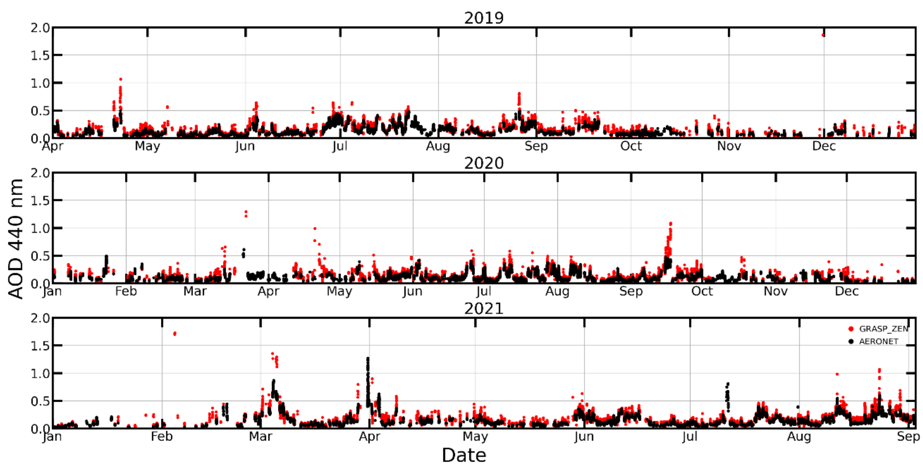

Figure 11. Time series evolution of aerosol optical depth (AOD) at 440 nm retrieved by GRASP-ZEN and by AERONET at Valladolid for all the ZEN-R52 available dataset (April 2019 to September 2021).

https://doi.org/10.5194/egusphere-2023-1040
Preprint. Discussion started: 1 June 2023

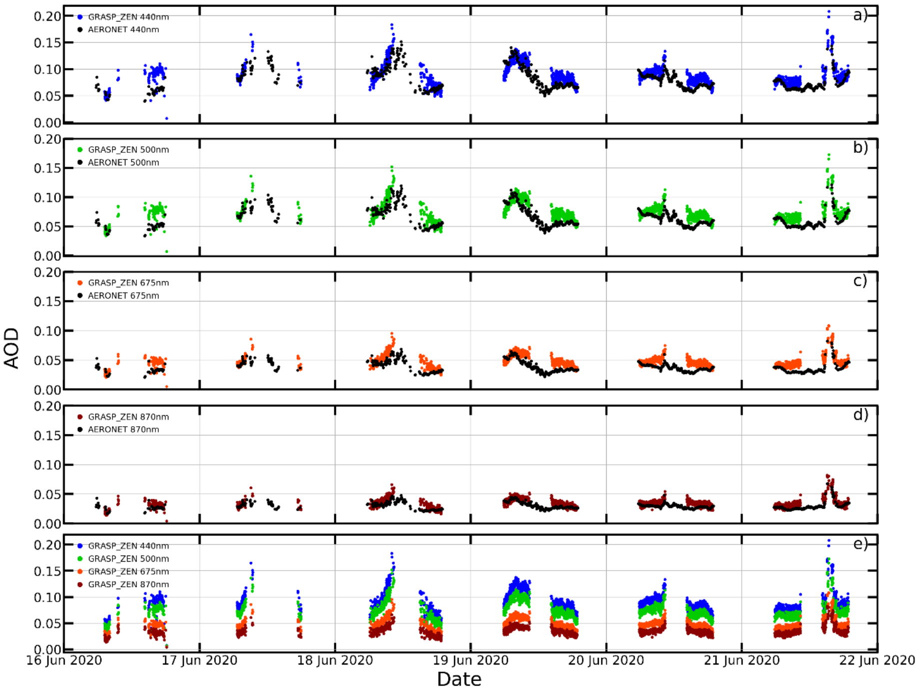

Figure 12. (a-d) Time series evolution of aerosol optical depth (AOD) at a) 440 nm, b) 500 nm, c) 675 nm and d) 870 nm retrieved by GRASP-ZEN and by AERONET at Valladolid for a week period in summer 2020 (16 to 22 June). (e) AOD retrieved by GRASP-ZEN for all ZEN-R52 channels plotted together.

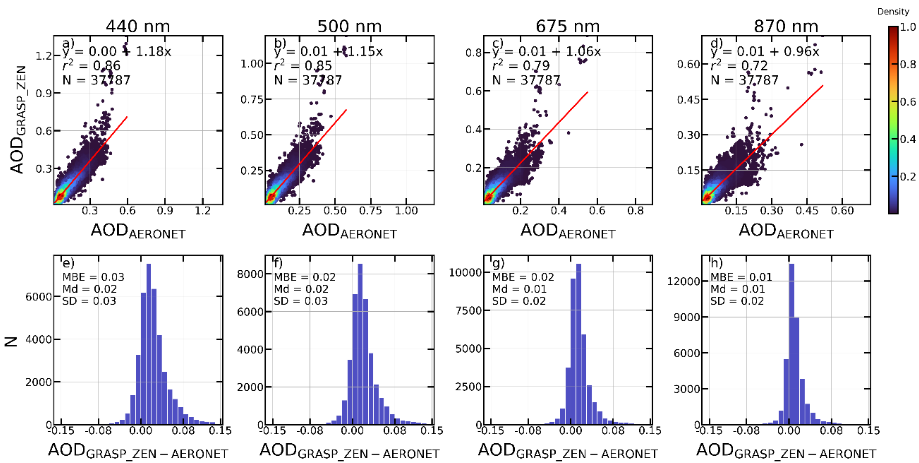

Figure 13. (a-d) Density scatter plots of the AOD retrieved by GRASP-ZEN (AOD_{GRASP_ZEN}) against coincident measurement from AERONET ($AOD_{AERONET}$) at a) 440 nm, b) 500 nm, c) 675 nm and d) 870 nm. Linear fit (red line), its equation, determination coefficient (r^2) and number of data pairs (N) are shown. (e-h) Frequency histograms of the absolute differences in AOD from GRASP-ZEN and AERONET at e) 440nm, f) 500nm, g) 675 nm and h) 870 nm. The mean bias error (MBE), median (Md) and standard deviation (SD) are also shown.

https://doi.org/10.5194/egusphere-2023-1040
Preprint. Discussion started: 1 June 2023

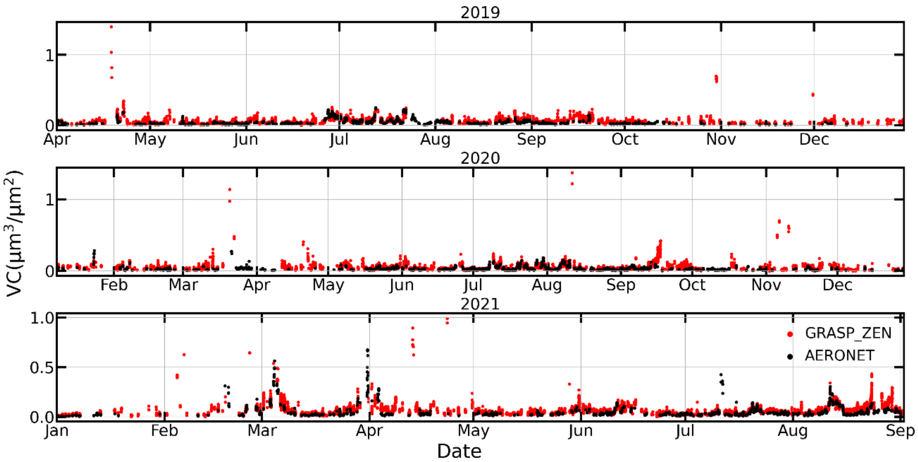

Figure 14. Time series evolution of the total volume concentration (VCT) retrieved by GRASP-ZEN and by AERONET at Valladolid for all the ZEN-R52 available dataset (April 2019 to September 2021).

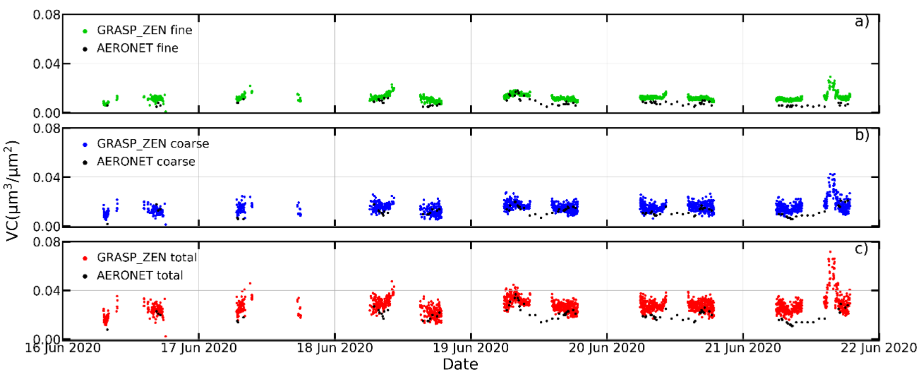

Figure 15. Time series evolution of volume concentration for fine (VCF) and coarse (VCC) modes and the total (VCT) retrieved by GRASP-ZEN and by AERONET at Valladolid for a week period in summer 2020 (16 to 22 June).

https://doi.org/10.5194/egusphere-2023-1040
Preprint. Discussion started: 1 June 2023

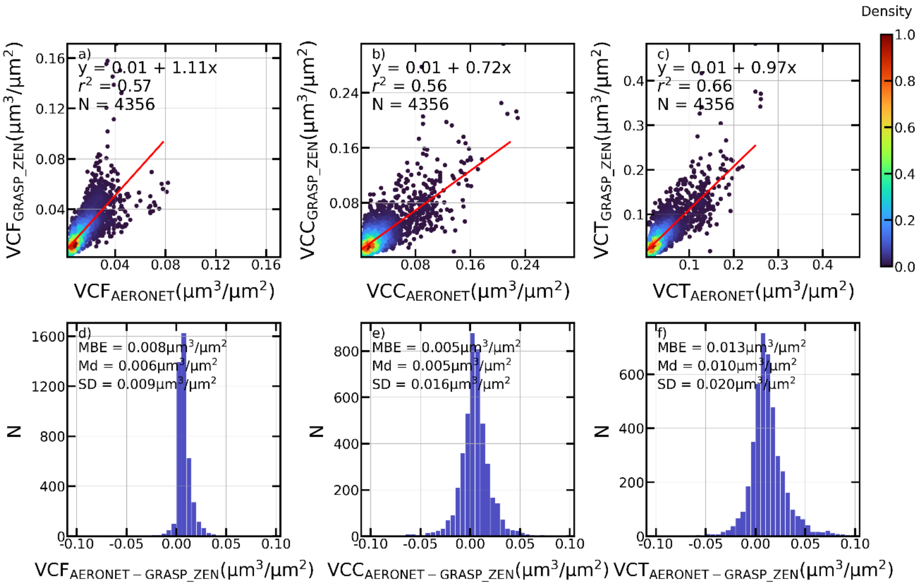

Figure 16. (a-c) Density scatter plot of the volume concentration for fine (VCF) and coarse (VCC) modes and total (VCT) retrieved by GRASP-ZEN against coincident retrievals from AERONET. Linear fit (red line), its equation, determination coefficient (r^2) and number of data points (N) are shown. (e-h) Frequency histograms of the absolute differences between both datasets. The mean bias error (MBE), median (Md) and standard deviation (SD) are also shown.